Intermediate Bents – Calculation of Restraint Factor

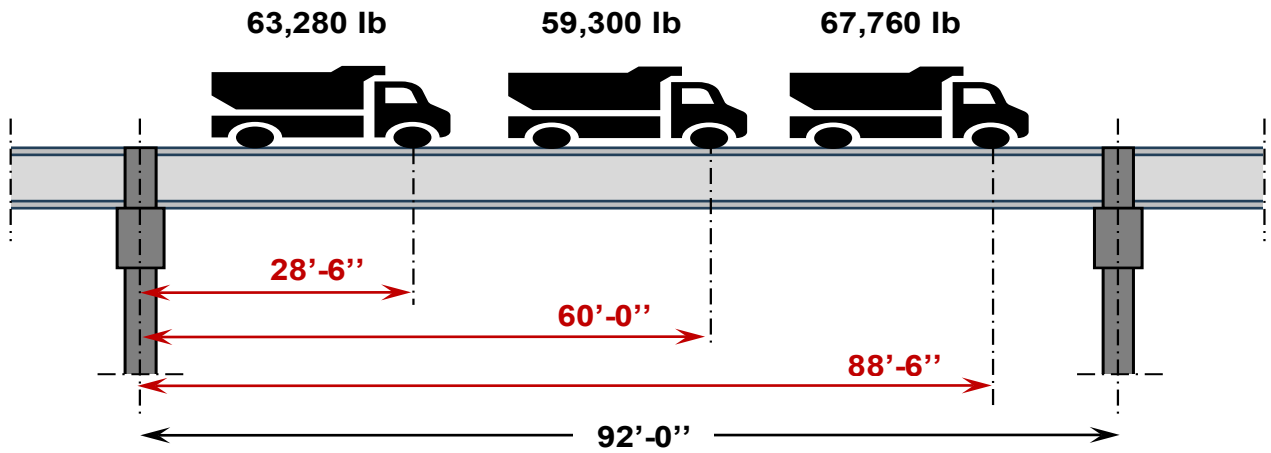

June 2024
Final Report

Project number TR202203
MoDOT Research Report number cmr 24-004

PREPARED BY:

Sarah Orton

Alaaeldin Elsisi

David Barrett

Cory Imhoff

Narek Galustanian

Mohamed Elshazli

Olivia Bommelje

University of Missouri-Columbia

PREPARED FOR:

Missouri Department of Transportation

Construction and Materials Division, Research Section

Technical Report Documentation Page

1. Report No. cmr 24-004	2. Government Accession No.	3. Recipient's Catalog No.
4. Title and Subtitle Intermediate Bents – Calculation of Restraint Factor		5. Report Date June 2024 Published: June 2024
		6. Performing Organization Code
7. Author(s) Sarah Orton, https://orcid.org/0000-0002-7896-039X Alaaeldin Elsisi, https://orcid.org/0000-0001-8190-6100 David Barrett, Cory Imhoff, Narek Galustanian, Mohamed Elshazli, Olivia Bommelje		8. Performing Organization Report No.
9. Performing Organization Name and Address University of Missouri Columbia E2509 Lafferre Hall, Columbia, MO 65201 Southern Illinois University-Edwardsville 61 Circle Drive Edwardsville, IL 62026 HDR, Inc. 4435 Main Street, Suite 1000, Kansas City, MO 64111-1856		10. Work Unit No. (TRAIS)
		11. Contract or Grant No. MoDOT project # TR202203
12. Sponsoring Agency Name and Address Missouri Department of Transportation (SPR-B) Construction & Materials Division P. O. Box 270 Jefferson City, MO 65102		13. Type of Report and Period Covered Final Report (September 2022-June 2024)
		14. Sponsoring Agency Code
15. Supplementary Notes Conducted in cooperation with the U.S. Department of Transportation, Federal Highway Administration. MoDOT research reports are available in the Innovation Library at https://www.modot.org/research-publications.		
16. Abstract This report investigates the restraint at the top of the column of non-integral intermediate bents with closed diaphragms, a common connection configuration utilized by the MoDOT. Although closed diaphragms inherently possess some level of rotational restraint, the current design approach considers this type of connection as free, resulting in the use of design k-factors of 2.1. However, rotational restraint significantly influences the k-factor. Utilizing an integration of experimental and numerical analyses, the study determined the approximate level of restraint of these types of intermediate bents. The main source of rotational flexibility was in the diaphragm to bent cap connection. A parametric analysis showed that the dowel bar area, diaphragm width, and skew angle were all parameters that needed to be considered in the simplified equation to predict the rotational restraint developed as part of this study. A comparison of the simplified equation to predict rotational restraint showed at most a 10% difference compared to that found in the FE models. Calculations of the k-factors, using a simplified bilinear equation, showed k-factors less than the assumed 2.0 theoretical value for fixed-free columns (on average 1.5), and in the case of the steel column bridge a k-factor of only 1.2. A procedure for analyzing telescoping columns was also formulated in which an effective moment of inertia can be used to treat the column as a uniform diameter. Three examples showed that the use of rotational restraint increased the buckling capacity of the concrete column by 24% to 40%. However, for steel HP columns this increase was most significant at 62%, which changed the controlling buckling mode to the weak axis direction. If buckling capacity controls the design of the column this could result in a potential cost savings of 20 to 30% of the column cost. The work culminates in a suggested design procedure to use rotational restraint in the design of intermediate bent bridge columns.		
17. Key Words Intermediate bent, Column, Rotational restraint, k-factor	18. Distribution Statement No restrictions. This document is available through the National Technical Information Service, Springfield, VA 22161.	

19. Security Classification (of this report) Unclassified	20. Security Classification (of this page) Unclassified	21. No. of Pages 81	22. Price

Form DOT F 1700.7 (8-72) Reproduction of completed page authorized

Intermediate Bents – Calculation of Restraint Factor

By
Sarah Orton, Narek Galustanian, Mohmed Elshazli, Olivia Bommelje
University of Missouri Columbia

Alaaeldin Elsisi
Southern Illinois University Edwardsville

Cory Imhoff, David Barrett
HDR

Prepared for
Missouri Department of Transportation

June 2024

Final Report

cmr 14-004

Copyright

Disclaimer

Acknowledgements

The authors would like to thank the Missouri Department of Transportation and the Missouri Center for Transportation Innovation for sponsoring this research. The authors would also like to thank the Missouri Department of Transportation Technical Advisory Committee for their assistance in the research. In addition, the authors would like to thank University of Missouri Lab Technician Chris Strehl for his help with the experimental work.

Table of Contents

List of Tables

List of Figures

List of Equations

List of Abbreviations and Acronyms

DIC…….Digital Image Correlation

FE……Finite Element

LRFD ..... Load and Resistance Factor Design

LVDT…….Linear Variable Differential Transformer

MoDOT ..... Missouri Department of Transportation

Executive Summary

MoDOT currently uses a k-factor of 2.1 for out-of-plane bending to evaluate the buckling resistance of non-integral intermediate bent columns in prestressed concrete superstructures (assuming a fixed-free condition). However, the restraint provided by longitudinal girders at the top of a column provides additional resistance to the buckling of the column and may allow a reduction in the k-factor to as low as 1.2 (for a fixed – rotationally restrained condition). The project determined the actual level of restraint at the top of the columns so that more accurate values of k-factors can be used. The project detailed Finite Element (FE) models (bridges A7957, A8697, and A8279) using ANSYS workbench. The detailed FE models considered the standard design details including the shear keys, dowel bars, roofing felt bond breaker between the diaphragm and bent cap, and joint filler at the edge of the diaphragm. The main source of rotational movement was found to be the connection between the bent cap and diaphragm. The A8697 bridge and the A7957 bridge were used for the FE validation.

Experimental testing was conducted on bridge A8697 via loaded dump trucks. The movements of the bridge were recorded via Digital Image Correlation (DIC) and Linear Variable Differential Transformers (LVDT). The DIC data showed good accuracy in the horizontal direction but was less accurate in the vertical direction due to possible movements in the camera. The DIC rotation data showed that the girder and diaphragm rotated together with about 10 times more rotation than the bent cap and was consistent with the FE model results showing most of the rotational flexibility due to the bent cap to diaphragm connection. The LVDT data was consistent across all three test runs and matched the FE model predictions for the bent cap and loaded side girder deflections. Overall, the experimental results generally matched the results of the FE model, but there was difficulty in obtaining precise experimental data due to noise.

A parametric analysis was performed to determine the influence of several key parameters on the rotational restraint at the top of intermediate bent columns. The results showed that the dowel bar area, diaphragm width, and skew angle were all parameters that needed to be considered in the simplified equation to predict the rotational restraint. The girder length and stiffness were found not to be important, and the connection interface is assumed part of standard design. The concrete modulus is important but considered to be a constant for 4000 psi concrete. The column length and stiffness as well as the bent cap length will be directly considered in the k-factor equation.

The project proposes a simplified equation using parameters of dowel bar area, diaphragm width, and skew angle to estimate the level of rotational restraint based on the dowel bar area, diaphragm width, and skew angle. A comparison showed that the predicted rotational restraint was within 10% of that found in the FE models. Using this equation, the k-factor can be determined and buckling analysis of the column can be conducted. Calculations of the k-factors for the modeled bridges showed k-factors less than the assumed 2.0 theoretical for a fixed-pin column with average values around 1.5 and in the case of the steel column bridge a k-factor of only 1.2. A procedure for analyzing telescoping columns was also formulated in which an effective moment of inertia can be used to treat the column as a uniform diameter. Three

examples showed that the use of rotational restraint increased the buckling capacity of the concrete column by 24% to 40%. However, for steel HP columns this increase was the most significant at 62% which changed the controlling buckling mode to the weak axis direction. If buckling capacity controls the design of the column, this could potentially result in a cost savings of 20 to 30% of the cost of the bridge columns.

The work culminates in a suggested design procedure to use rotational restraint in the design of intermediate bent bridge columns.

Chapter 1. Introduction

MoDOT uses Load Factor and Resistance Design (LRFD) for bridge structures, and the Engineering Policy Guide article 751.31 contains standards for column design in closed concrete intermediate bents. Currently, per 751.31.2.4 a k-factor of 2.1 is used for evaluating the buckling resistance of non-integral intermediate bent columns for out of plane bending in prestressed concrete superstructures, assuming a fixed-free condition. However, the presence of the cast in place diaphragm and dowel bars as well as longitudinal girders at the top of a column provides additional resistance to buckling, potentially allowing a reduction in the k-factor to 1.2, indicating a fixed-rotationally restrained condition. This project aims to determine the actual level of restraint at the top of the columns so that more accurate values of k-factors can be used. To do so, refined Finite Element (FE) models of prestressed concrete bridges, validated with experimental field data, were developed to evaluate the level of rotational restraint. With the approximate value of rotational restraint, a simplified formula was developed to estimate the rotational restraint and determine a k-factor for column buckling design. By reducing uncertainty in effective buckling length and enabling the design of more slender intermediate bents without compromising stability, this research leads to potentially significant cost-savings.

Research Objectives

The primary goal of this project is to assess the level of restraint that takes place at the top of an intermediate bent in a prestressed concrete superstructure. The level of restraint is critical in determining the optimal k-factor for column design. The project includes a thorough analysis of non-integral intermediate bent end restraint, considering a wide range of parameters, including dowel bar area, diaphragm width, skew angles, column length and stiffness, girder length and stiffness, and connection interface properties. The project aims to achieve several outcomes, including the development of a simplified equation to estimate rotational restraint for this type of connection and an equation for determining k-factors for column design. Additionally, the study considers telescoping columns and aims to outline potential cost savings by analyzing designs for concrete and steel bridge columns with and without modified k-factors.

Research Tasks

- Conduct a thorough review of existing literature related to rotational restraint at bridge bents
- Develop and validate a finite element (FE) model to evaluate the amount of rotation at intermediate bents
- Perform experimental tests on a bridge structure utilizing LVDT’s and Digital Image Correlation (DIC) techniques to capture the deflection and rotation of an intermediate bent; the results will also be utilized to validate the FE models
- Derive simplified equations for rotational restraint and k-factors to be used in the design of non-integral circular reinforced concrete intermediate bent columns

- Evaluate rotational restraint for H-Pile (HP) steel columns
- Evaluate k-factors for telescoping columns

Report Overview

The report is organized as follows: **Chapter 2** provides the relevant background related to rotational restraint at intermediate bridge bents, summarizing key findings and identifying gaps in knowledge that the current study aims to address. **Chapter 3** outlines the development of the detailed FE models used in this study using ANSYS workbench. **Chapter 4** provides the testing procedure, including setup, instrumentation, and data acquisition. It also presents the results of the experimental bridge test and compares the results to the FE model for validation. **Chapter 5** contains the parametric analysis conducted via the FE models to isolate the parameters that most influence the degree of rotational restraint and presents the simplified formula to predict rotational restraint. **Chapter 6** presents the evaluation of the k-factor and possible cost savings from using the revised k-factor calculations as well as potential design recommendations and assumptions.

Chapter 2. Background

Typical prestressed concrete bridge design consists of a sub-structure including the bridge columns and bent cap beam. This is connected to the bridge superstructure (precast girders and cast-in place deck) through a cast-in place concrete diaphragm – see **Figure 2-1**. The details of how the diaphragm is connected to the bent cap beam vary depending on the state regulations. In this report we will consider the typical closed diaphragm as specified in the MoDOT EPG (Missouri Department of Transportation, 2023) that consists of a shear key and dowel bars with concrete poured the full height of the diaphragm, **Figure 2-2**. This type of diaphragm configuration is preferred when future maintenance of the bearing pads is not anticipated. The closed nature of the diaphragm also reduces maintenance needs by minimizing the penetration of contaminants (de-icing salts) that can deteriorate the ends of the prestressed girders. An alternative to the closed diaphragm is the open diaphragm, in which concrete is not cast the full depth to the bent cap. However, this type of diaphragm is more likely to behave as a free end, lacking rotational restraint, and therefore, it is not studied in this report.

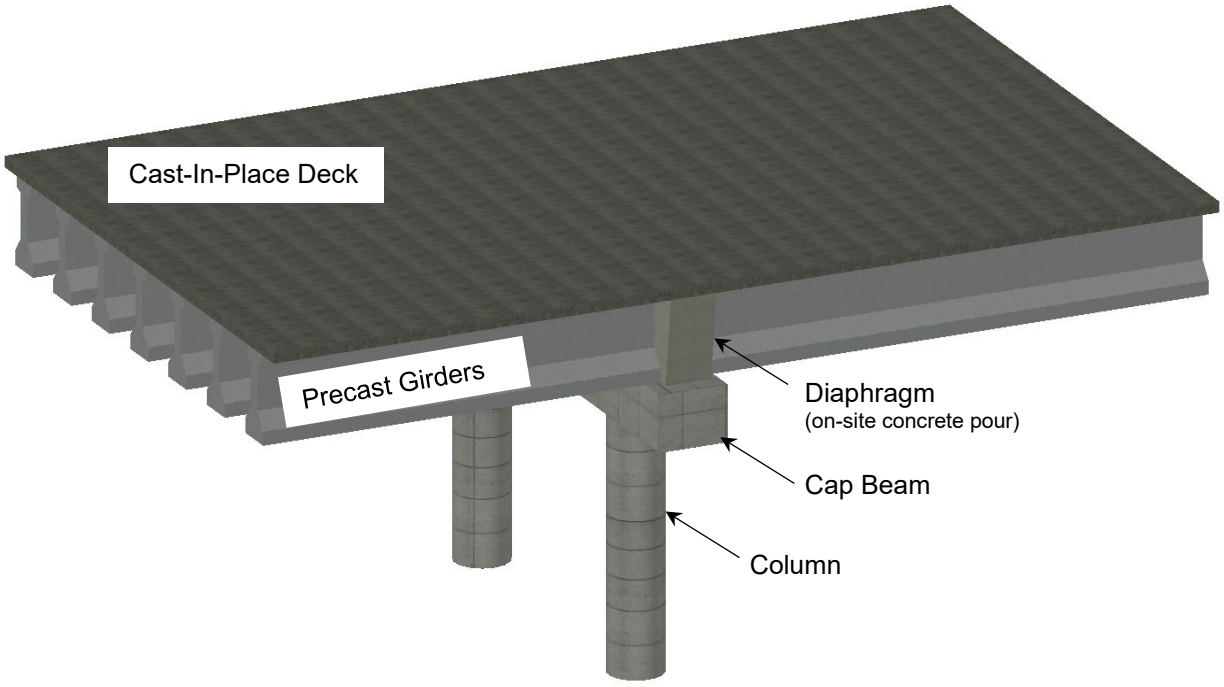

Figure 2-1. Typical intermediate bent connection

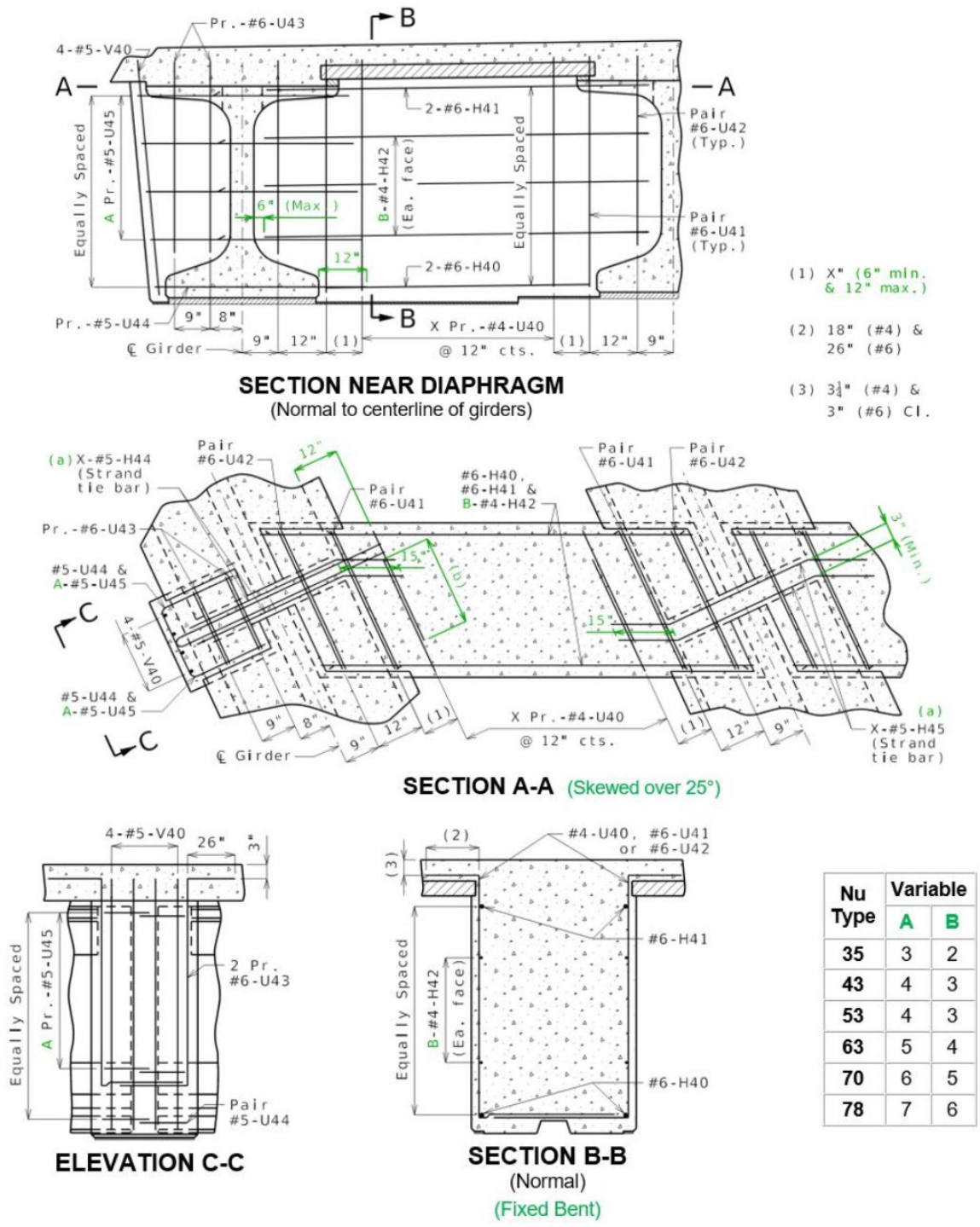

Nu Type	Variable	
	A	B
35	3	2
43	4	3
53	4	3
63	5	4
70	6	5
78	7	6

Figure 2-2. Closed Intermediate Diaphragm Elevation and Cross-Section (MoDOT EPG 751.22.3.7)

Diaphragm Connections

The integration of cast-in-place diaphragms within intermediate bents serves as an important connection between the girders of adjacent spans and the superstructure's connection to the pier cap (Hou & Chen, 2017). This connection is critical for ensuring the overall stability and structural integrity of the bridge. Three typical design configurations of bent connections have been introduced; isolated, integral, and non-integral connections (Hastak et al., 2003; Miller, 2004). Isolated connections or open diaphragms are formed by placing continuous girders and diaphragms on bearing pads that are not directly attached to the substructure (Hou & Chen, 2017). These types of connections provide little moment restraint and are not studied in this report. Integral connections provide a strong, fully rigid link between the superstructure and pier cap. Integral pier caps are designed to be monolithic with the adjacent structural elements, ensuring seamless load transfer and enhanced structural performance. These connections are particularly advantageous in seismic regions, as they can improve the overall seismic resilience of the structure (Nielson, 2005; Nielson & DesRoches, 2007). As the connection is designed to transfer moment, the restraint has already been evaluated and researched in several previous studies. Unlike integral connections, which are designed to form a continuous and uninterrupted load path between structural members, non-integral connections (such as the closed diaphragm studied here) are assumed to have limited moment resistance (Hou & Chen, 2017).

For integral connections, numerous approaches have been proposed to establish a moment connection between the superstructure and cap beam. Most of these systems require the development of a connection mechanism between the girder and diaphragm to resist the bending moment due to the applied loading. Early investigations explored the utilization of bent bars (see **Figure 2-3**) (Hanson, 1960; Kaar et al., 1960; Mattock, 1961). In this configuration, hooked, mild reinforcing bars are embedded at the end of precast girders. The hooks are then integrated into the diaphragm. Alternatively, the bent-strand connection method was introduced (Abdalla et al., 1993; Clark & Sugie, 1997; Salmons, 1974), where a specified length of prestressing strand is left protruding from the girder end upon de-tensioning. The strand is then bent into a 90-degree hook and embedded within the diaphragm (see **Figure 2-3**). The Missouri Department of Transportation (MoDOT) conducted a study on this connection type in the 1970's (Salmons, 1974; Salmons & McCrate, 1973), and a design methodology was proposed for developing positive moment connections utilizing bent strands. Additional approaches to positive moment connections include the use of straight bars, welded bars, extending reinforcement through the web of the girders into the diaphragms, adopting mechanical strand connectors, and implementing partial diaphragms to pre-compress the section (Abdalla et al., 1993; Snyder, 2010; Tadros et al., 1993; Thonstad et al., 2021).

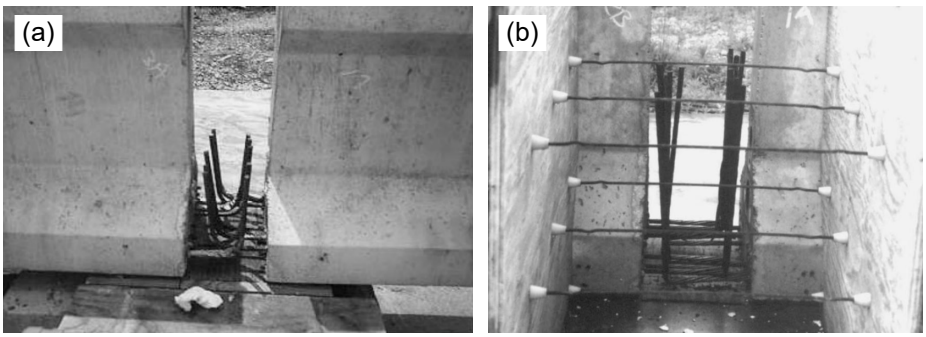

Figure 2-3. Continuity connection at internal support;
a) bent bars connection, b) bent-strand connection

The previous research demonstrates that these connections show varying levels of moment restraint across different loading conditions. Research on integral superstructures primarily focuses on their seismic response. In (Peggar, 2014), two different details for precast girders forming fixed girder-to-cap connections were investigated. Through a comparison of the moment-rotation responses of these connections, it was concluded that they offer sufficient rotational restraint for high seismic demands, thus presenting a cost-effective and dependable solution for bridge construction in seismic regions. Similarly, (Holombo et al., 2000) studied the seismic performance of precast prestressed concrete spliced-girder bridges with integral column-superstructure connections. The research involved subjecting two 40% scale model bridge structures to fully reversed simulated seismic forces and longitudinal displacements. The study aimed to verify a design methodology for such bridges under seismic loads, with a specific focus on the force-displacement hysteresis behavior of the girder-column connections. The results exceeded design requirements, demonstrating the effectiveness of the integral connection design in enhancing seismic resilience.

In the context of closed diaphragms, presuming them to be free ends may be excessively conservative. Traditionally, such connections are idealized using fixed, pinned, or roller supports. However, depending on the specific design and construction details, some physical connections can actually behave somewhere between two idealized connections. Various factors contribute to the level of rotational restraint experienced at intermediate bents. The k-factor equation used for column design accounts for parameters such as column length and stiffness, reflecting their influence on the structural resistance to buckling. On the other side, the length and stiffness of girders may impact rotational restraint. Additionally, the width of the diaphragm, skew angles, and the ratio of dowel bar reinforcement are expected to influence the rotational stiffness of the connection. Understanding these interactions is essential for accurately assessing the level of rotational restraint and optimizing the design of closed diaphragms in prestressed concrete bridge structures.

Effect of Connection Rotational Stiffness

The accurate characterization of connections is critical for ensuring structural reliability and stability. While much research work has been done to determine the strength limit states of

different types of connections (Grauvilardell et al., 2005; Kanvinde et al., 2012a), there is a clear gap in addressing rotational flexibility, particularly concerning the end restraints of intermediate bents. The ratio of the rotational stiffness of connections to the flexural stiffness of the members influences the critical buckling load. Higher rotational stiffness in connections relative to member stiffness can increase the critical load, thus delaying or preventing buckling and resulting in a lower k-factor. Experimental and analytical approaches can be used to determine rotational stiffness in structural connections.

Picard & Beaulieu (1985) experimentally investigated the degree of fixity of column-base connections. The experimental setup involved the application of a lateral load to a steel column using a hydraulic jack positioned at a distance *(L)* from the top of the base plate, as shown in **Figure 2-4** (Picard & Beaulieu, 1985a). Dial gauges were used to measure the rotation of the column, and flexibility factors (λ) were calculated as the ratio of the measured rotation (θ) to the applied bending moment $(M = F \times L)$. The fixity factor (γ) was then determined using the equation provided by (Brun, 1976),

Equation 1. For a perfectly fixed connection, this equation yields a fixity factor of 1.0. The study revealed that the analysis method employed to find the ultimate moment capacity, assuming a perfectly rigid base connection, was conservative. Further research used a similar experimental approach to determine the flexibility of column-base connections, aiming to improve the design practice (Astaneh et al., 1992; Gomez et al., 2010; Picard & Beaulieu, 1985b).

$$\gamma = \frac{1}{1 + \frac{3EI\lambda_o}{L}}$$

Where:

γ = the column fixity

E = the modulus of elasticity of the column

I = the bending moment of inertia

λ_o = the flexibility factor at the connection (x = 0)

L = the column length

Equation 1. The Fixity Factor (Brun, 1976)

Earlier research studies established the component analytical approach, which assumes a linear strain distribution throughout the length of the base plate (Balut & Moldovan, 1997; Jaspart & Vandegans, 1998; Salmon et al., 1957; Sato, 1987; Wald et al., 1996). This assumption ensures deformation compatibility across various components at the connection. However, this method assumes rigid components and ignores their interactions. Therefore, advanced methods were introduced to incorporate the interactive dynamics among components (Ermopoulos & Stamatopoulos, 1996; Melchers, 1992). Furthermore, (Kanvinde et al., 2012b) developed an approach to determine the flexural stiffness of column base connections under combined flexural and axial loads. This approach was validated against previous experimental data,

demonstrating reasonable accuracy in predicting flexural stiffness, particularly under highly eccentric loading.

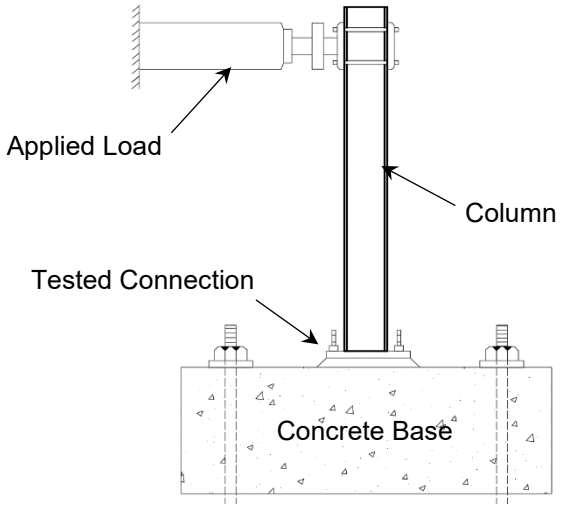

Figure 2-4. Typical experimental setup for determining rotational stiffness of connections

Effective Buckling Length

The design of columns heavily relies on Leonhard Euler's Theory of Elastic Buckling. Euler's Theory of Elastic Buckling addresses the axial compression stability of slender columns by establishing a critical load, known as the Euler buckling load, which represents the maximum axial load before the start of buckling instability, **Equation 2**.

$$P_{cr} = \frac{\pi^2 EI}{(kL)^2}$$

Where:

E = the modulus of elasticity of the material

I = the bending moment of inertia

L = the length of a member

k = the effective length constant

Equation 2. Euler's Equation of Elastic Buckling

The k-factor is a non-dimensional value that relates the elastic buckling load (P_{cr}) of an end-restrained column to the Euler buckling load (P_e) by creating an effective length kL. Therefore, the k-factor can be found as:

$$k = \sqrt{\frac{P_e}{P_{cr}}} = \sqrt{\frac{\pi^2 EI}{L^2 P_{cr}}}$$

Where:

E = the modulus of elasticity of the material

I = the bending moment of inertia

L = the length of member

k = the effective length constant

Equation 3. Effective Length Factor (k-factor)

The level of restraint at the top and bottom of the column can be used to determine the k-factor and effective length of the column. A generic level of restraint is demonstrated by the rotational springs in

Figure 2-5. The exact value of the k-factor can be solved through eigenvalue analysis in **Equation 4**. The level of restraint at the top of the column (R_{kB}) is directly related to the k-factor. The restraint (R_{kB}) is based on the beam stiffness and length (EI/L) as well as the details connecting the beams to the columns.

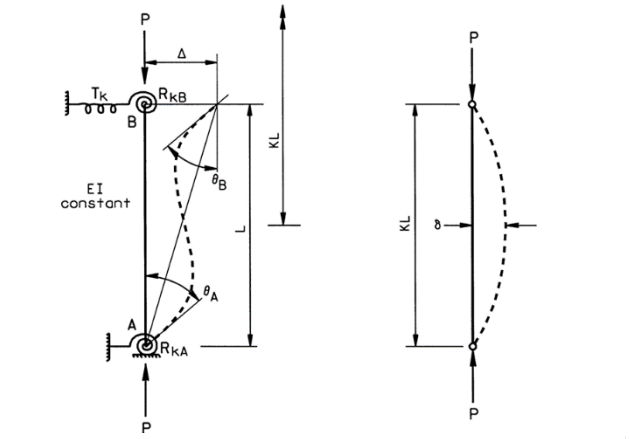

(a) End-restrained Column (b) Pin-ended Column

Figure 2-5. Generic restraint in column

$$det\begin{vmatrix} C + \frac{R_{kA}L}{EI} & S & -(C+S) \\ S & C + \frac{R_{kB}L}{EI} & -(C+S) \\ -(C+S) & -(C+S) & 2(C+S) - \left(\frac{\pi}{K}\right)^2 + \frac{T_k L^3}{EI} \end{vmatrix}$$

Where:

C = the stability function $C = \frac{(\pi/K)\sin(\pi/K) - (\pi/K)^2 \cos(\pi/K)}{2 - 2\cos(\pi/K) - (\pi/K)\sin(\pi/K)}$

S = the stability function $S = \frac{(\pi/K)^2 - (\pi/K)\sin(\pi/K)}{2 - 2\cos(\pi/K) - (\pi/K)\sin(\pi/K)}$

Equation 4. Eigenvalue analysis of the k-factor (Duan & Chen, 1999)

When **Equation 4** is solved for a variable column length (L) and stiffness (EI), **Figure 2-6** is produced. Therefore, the k-factor to be used in the buckling analysis can be reduced to a function of the rotational restraint at the diaphragm-bent cap-girder connection (R_{kb}) as well as the column length and stiffness (EI/L). As expected, the k-factor is bound between 2.0 (free end) and 1.0 (fixed end). This report is focused on evaluating the rotational restraint at the top of the column.

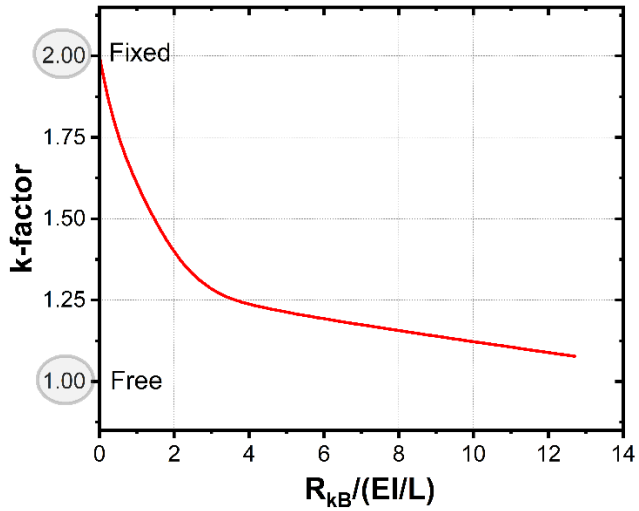

Figure 2-6. K-factor for variable rotational restraint (R_{kb}) and column length and stiffness (EI/L)

Effect of Column Stiffness

The column length and stiffness have a direct effect on the k-factor for buckling analysis, as shown in **Figure 2-6.** One way to understand the importance of the column length and stiffness is to look at an alignment chart, as shown in **Figure 2-7**. The connection at the top of the column can vary between pinned ($G_A = \infty$) and fixed ($G_A = 0$), leading to a k-factor ranging between 2.0 and 1.0. The factor G_A represents the ratio between the column length and stiffness and the rotational restraint. Therefore, as the column becomes longer or more flexible, the rotational restraint needs to be less to maintain the same G_A and k-factor. Conversely, as the column becomes shorter and stiffer, the rotational restraint needs to be greater to maintain the same G_A and k-factor. This means that column length and stiffness have a significant effect on the k-factor and the needed rotational restraint level. However, as

illustrated in **Figure 2-6**, the effect of the column length and stiffness can be directly accounted for in the equation for the k-factor. Therefore, this report will focus on evaluating the rotational restraint at the top of the column.

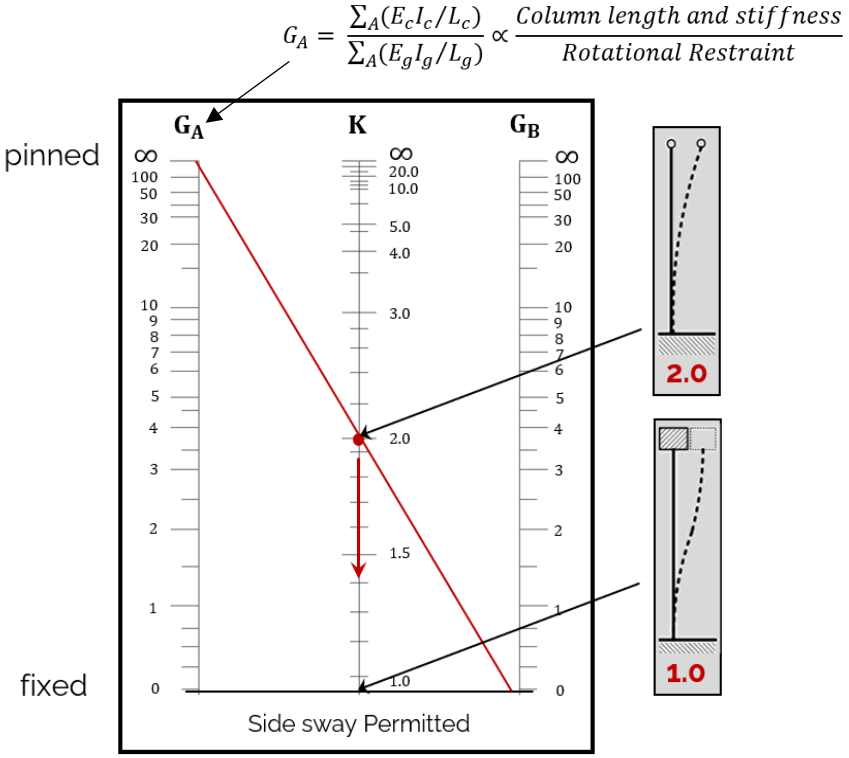

Figure 2-7. Alignment chart to illustrate importance of column length and stiffness on k-factor

Digital Image Correlation (DIC) Measurements

To evaluate the rotational restraint at the top of the column, an experimental test will be conducted using a Digital Image Correlation (DIC) system. DICs have emerged as invaluable tools in the field of experimental mechanics and structural health monitoring, primarily due to their ability to accurately measure displacements and strains from a distance. DIC has shown remarkable capabilities comparable to traditional instruments such as Linear Variable Differential Transformers (LVDTs) and high-speed cameras. Furthermore, DIC may be used for accurately validating Finite Element (FE) models. However, it is uncertain how accurate the DIC measurement will be in the field from a distance. In experimental mechanics, DIC has demonstrated its efficacy in reliably measuring fracture mechanical parameters and identifying non-visible cracking. Similarly, in structural health monitoring applications, DIC offers a versatile solution for damage quantification, crack detection, and long-distance bridge deflection measurements.

Research conducted underscored the potential of DIC in structural health monitoring of bridges (Nonis et al., 2013). Their study validated DIC's capability in detecting non-visible cracking, quantifying concrete spalling, and monitoring long-term strain on structures. Additionally, (Desai, 2016) investigated the smallest detectable strain using DIC technology on a replica

beam-column moment connection. The study concluded that DIC could accurately capture strains as small as 0.03% (0.0003 strain), highlighting its sensitivity and precision in strain measurement. Furthermore, (Murray, 2013a) explored the application of DIC for monitoring rail displacements and reinforced concrete bridge displacements. Unlike traditional instruments, DIC proved capable of capturing both vertical and horizontal rail displacements and thus able to discern rotations. Additionally, (Bell et al., 2015a) utilized DIC measurements on a steel-girder bridge to calibrate a FE model and determine bridge load ratings. The study successfully demonstrated accurate deflection measurements, showcasing the potential of DIC in structural assessment. However, challenges such as noise interference in long-term strain monitoring have been encountered. Factors such as shallow camera angles, poor camera calibration, or excessive camera position shifts can introduce noise, rendering the DIC system unreliable for long-term strain monitoring (Bell et al., 2015b; Murray, 2013b; Nonis et al., 2013). Implementing advanced filtering approaches may help mitigate these challenges and ensure more accurate and reliable displacement measurements in DIC applications.

In this research, DIC was employed to measure both deflections and rotations of Bridge A8697 in Missouri. Utilizing DIC technology, the study aimed to gain insights into the level of restraint of the intermediate bent connection within the bridge structure as well as assess the accuracy of the DIC measurements in the field. Additionally, DIC may provide crucial data for validating FE models, enabling the performance of a parametric study to investigate the key parameters affecting rotational stiffness.

Summary

This research investigates the end restraint of non-integral intermediate bents, with a focus on a common connection configuration utilized by MoDOT. Among the different types of diaphragms, closed diaphragms, as specified in the MoDOT EPG 751.22.3.7 (Missouri Department of Transportation, 2023) are of interest in this study. These closed diaphragms are characterized by their full-height concrete pour, including shear keys and dowel bars, offering advantages such as reduced maintenance needs and improved durability. Although closed diaphragms inherently possess some level of rotational restraint, the current design approach considers this type of connection as free, resulting in the use of k-factors of 2.1. However, restraint arises from various sources, including the interaction between column stiffness, diaphragm width and stiffness, and the area of dowel bars. This rotational restraint significantly influences the k-factor. While experimental and analytical methods have been employed to determine the rotational stiffness of various connection types, none have addressed the end restraint of intermediate bents in prestressed bridges. In this type of connection, many parameters, including column stiffness, play a crucial role in determining the level of rotational restraint and, consequently, the k-factor. The interaction of these parameters complicates the assessment of rotational stiffness, requiring a thorough investigation of the key parameters contributing to the overall stiffness of the connection. Utilizing an integration of experimental and numerical analyses, the study seeks to determine the accurate level of restraint of these types of intermediate bents.

Chapter 3. Finite Element Modeling

This chapter presents the finite element modeling methodology followed in this research, which was specifically developed to investigate the end restraint of intermediate bents. The approach involved developing a finite element (FE) model using ANSYS workbench, subsequently validated through experimental testing (see **Chapter 4**). A parametric study was then conducted to investigate the effect of a wide range of parameters on the rotational stiffness of intermediate bent connections (see **Chapter 5**). Further details about the methodology, FE validation, and the comprehensive parametric study are discussed in this chapter.

FE Model Overview

In collaboration with MoDOT's Bridge Division and Construction & Materials Division, three bridges (A7957, A8697, and A8279) were modeled using ANSYS workbench. The A8697 Keytesville RTE 24 bridge over the Mussel Fork River and the A7957 bridge over the Maries River were used for the FE validation. Notably, the A8697 bridge was experimentally tested as part of this research, while the A7957 bridge had been previously tested by (Hernandez & Myers, 2016).

The detailed FE models considered a typical intermediate bent, as shown in **Figure 3-1** (A8697 used as the illustration). Different concrete components, including columns, bent cap beam, girders, deck, and diaphragm, were modeled using eight nodes solid elements (SOLID185). Additionally, all reinforcement and prestressing strands were modeled using beam elements (LINK 180), **Figure 3-2**. This model assumes that the reinforcing element is firmly attached to the base element, with no relative movement between the reinforcing element and the base allowed, thus representing a fully bonded constraint.

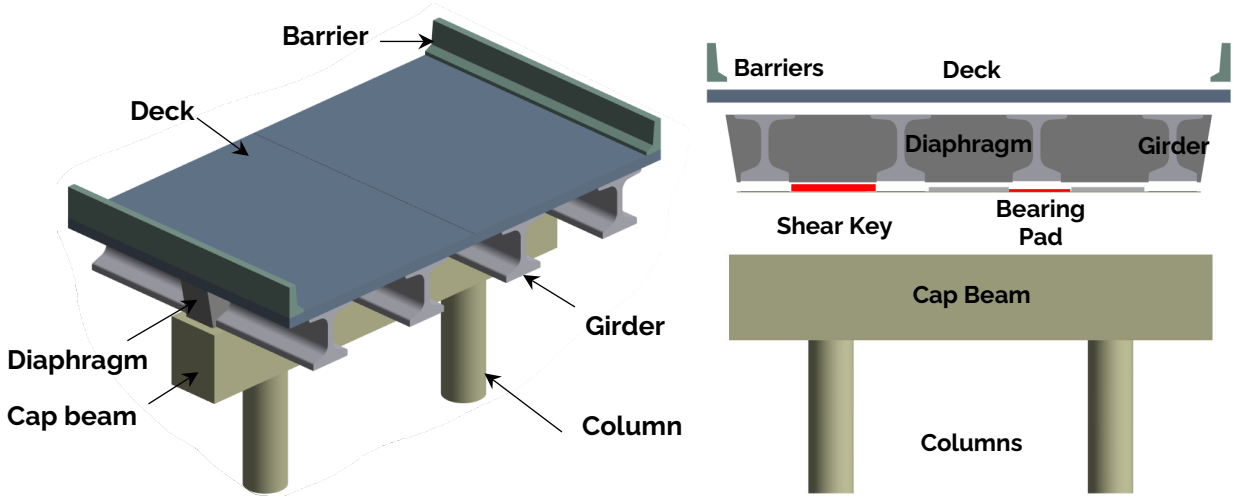

Figure 3-1. Typical FE model of the intermediate bent of the A8697 bridge

To have a comprehensive representation of the connection, shear keys, dowel bars, and bearing pads were modeled, as shown in **Figure 3-3**. The connection between the bent cap beam, and the diaphragm involved the use of shear keys modeled using SOLID185 elements. The surface between the diaphragm and bent cap utilized frictionless contact and was modeled using CONTA174 and TARGE170 elements. A layer of roofing felt is generally laid at this surface preventing bond. Dowel bars were incorporated between the bent cap and the diaphragm to transfer the loads, with the dowel bars modeled as beam elements and assumed to be fully bonded with the surrounding concrete. However, designers may need to check for development of the bars if utilizing the reduced k-factor. Furthermore, elastic bearing pads with a 14,000 psi stiffness were placed on the bent cap to support the girders, with these pads sharing nodes with the cap and employing frictionless contact with the girders using CONTA174 and TARGE170 elements. Joint filler around the edges of the cast-in-place diaphragm was applied with a 600 psi stiffness material.

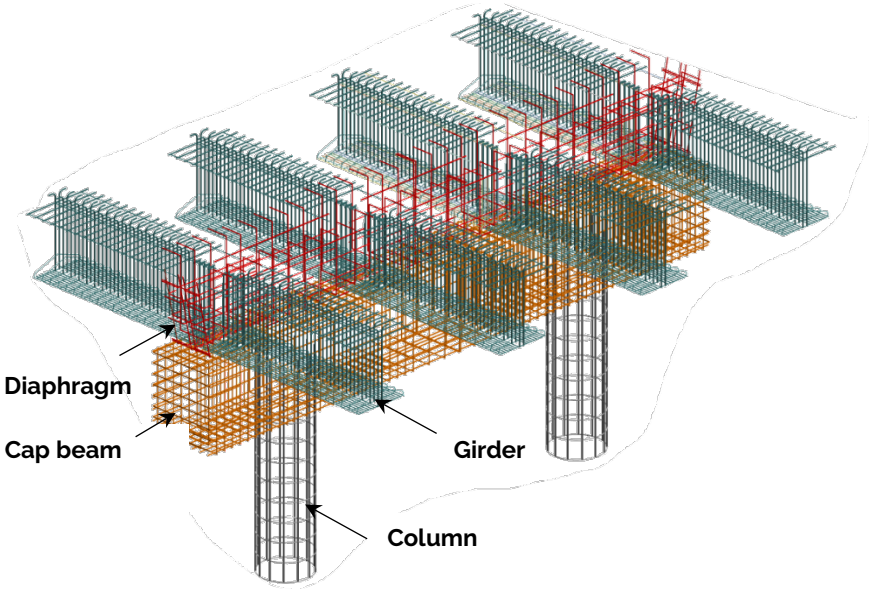

Figure 3-2. Reinforcement details of the intermediate bent

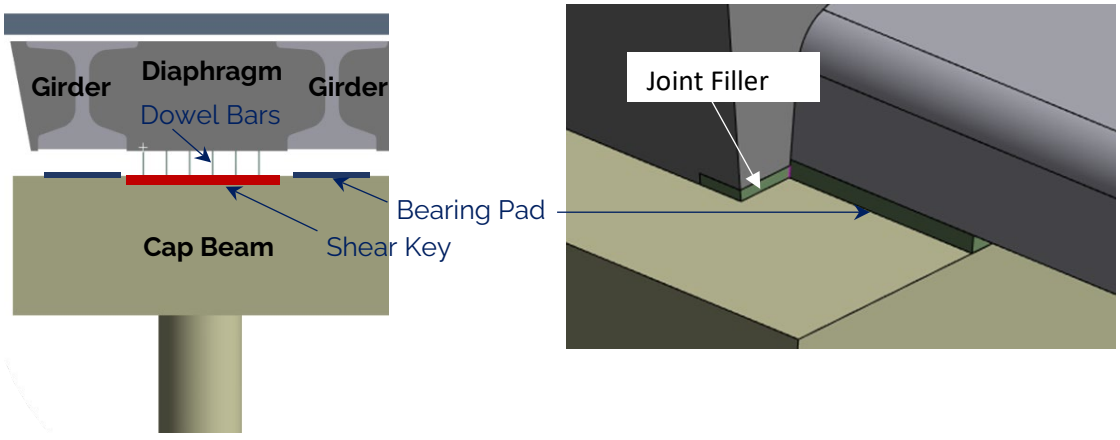

Figure 3-3. Detailed connection of the intermediate bent

The material properties for concrete and steel elements were defined according to the specifications outlined in the bridge design documentation. Concrete properties, including compressive strength, modulus of elasticity, and Poisson's ratio were used. The nonlinear behavior of concrete was considered using the Menetrey-Willam strain softening model (Menetrey & Willam, 1995). In addition, Grade 60 steel reinforcement and Grade 270 prestressing strands were modeled as elastic-perfectly plastic materials, including their behavior under tension and compression. The specific material properties used for the different bridge models are discussed in detail throughout this chapter.

To find the rotational stiffness of the connection (R_{kb}), horizontal displacement (δ) was applied at the bottom of the column, a distance (H) from the connection interface, with the resulting horizontal reaction (F_{HL}) recorded, as shown in **Figure 3-4**. Additionally, to account for bridge dead and live loads, an equivalent axial force (F_{VL}) was applied at the bottom of the column. The horizontal reaction (F_{HL}) obtained was used to determine the bending moment (M) at the connection, calculated as $(M = F_{HL} \times H)$. Furthermore, the angle of rotation (α) was calculated by taking the inverse tangent of the ratio of the lateral displacement (δ) to the column height (H). Utilizing these data points, a moment-rotation $(M - \alpha)$ curve was constructed, with the slope of the curve in the linear portion representing the rotational stiffness of the connection, as shown in **Figure 3-5**. In terms of boundary conditions, fixed ends were employed at the girder ends to simulate the constraints imposed by the rest of the bridge structure.

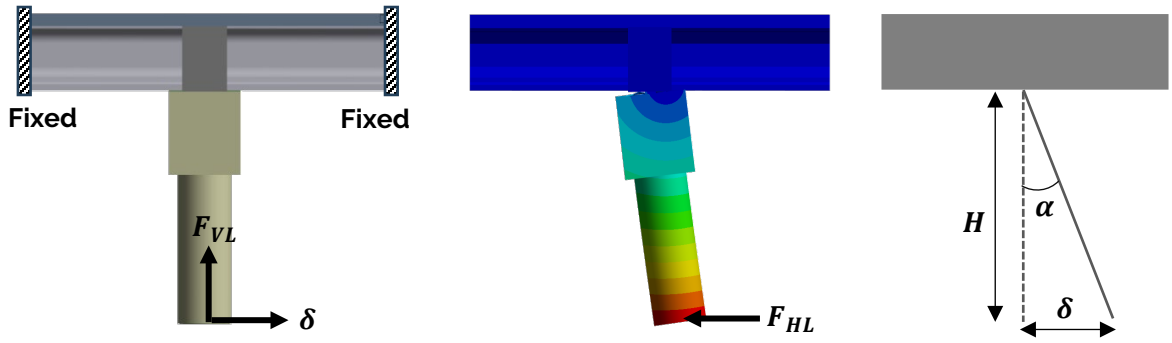

Figure 3-4. Methodology for evaluating rotational stiffness

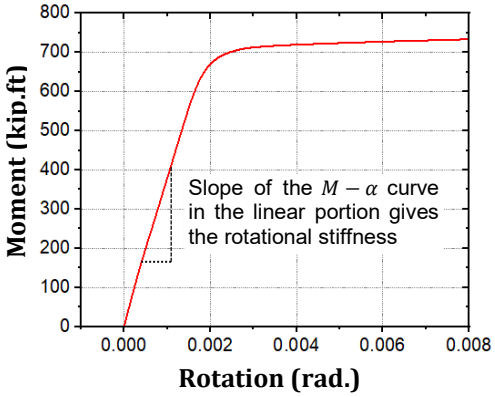

Figure 3-5. Typical moment-rotation $(M-\alpha)$ curve

A7957 Bridge

Bridge A7957, was included in the study to provide further validation and to explore additional parameters. This bridge is a three-span, continuous, precast prestressed (PC/PS) concrete bridge, supported by four NU53 PC/PS girders, **Figure 3-6**. The bridge deck consists of an 8.5 $in.$ reinforced concrete (RC) deck, with precast prestressed concrete panels used in the transverse direction between the top flanges of the girders and the RC deck. The superstructure is supported by two intermediate bents and two abutments, and the bridge has a skew angle of 30 degrees. **Figure 3-6** provides detailed illustrations of the bridge configuration. Closed intermediate diaphragms were used, with the diaphragms measuring 41 ft in length and 40.5 $in.$ in width, while the bent cap beams span 44 ft. Additionally, 24 #6 dowel bars, spaced at 12 $in.$, are used to connect the diaphragm with the bent cap. The supporting columns of the bridge stand at a height of 14.23 ft with a diameter of 4 ft on top of 4.5 ft diameter 52 ft long drilled shafts.

In a study conducted by (Hernandez & Myers, 2016), an instrumentation program was established to monitor the response of girders during the service life of Bridge A7957. The bridge was subjected to live load testing using dump trucks to produce maximum load effects. Subsequently, in this study, we developed a FE model and validated it against the experimental testing data. The FE model was constructed by utilizing consistent modeling criteria as discussed earlier, employing the same material properties as the actual bridge. Concrete materials were characterized by a density of 145 lb/ft^3 and a Poisson's ratio of 0.2. Elastic moduli were assigned to various components based on the compressive strength of the actual bridge as measured in (Hernandez & Myers, 2016): concrete columns, bent cap beams, diaphragms, and deck had a modulus of 4640 ksi, while girders were assigned an elastic modulus of 6525 ksi. Reinforcement elements were modeled with a density of 490 lb/ft^3 and an elastic modulus of 29,000 ksi. Grade 60 steel was used for steel rebar and dowel bars, while low-relaxation grade 270 was used for the prestressing strands.

The FE model showed a mid-span deflection of 0.288 $in.$ (**Figure 3-7**), demonstrating good agreement with the experimental result of 0.320 $in.$ After the validation, the rotational stiffness was calculated as demonstrated earlier in **Figure 3-4**. The FE model showed a rotational

stiffness (R_{kb}) of 552,474 $kip.ft/rad$. This rotational stiffness will serve as one of the key models in the final analysis to demonstrate the behavior of intermediate bent end connections.

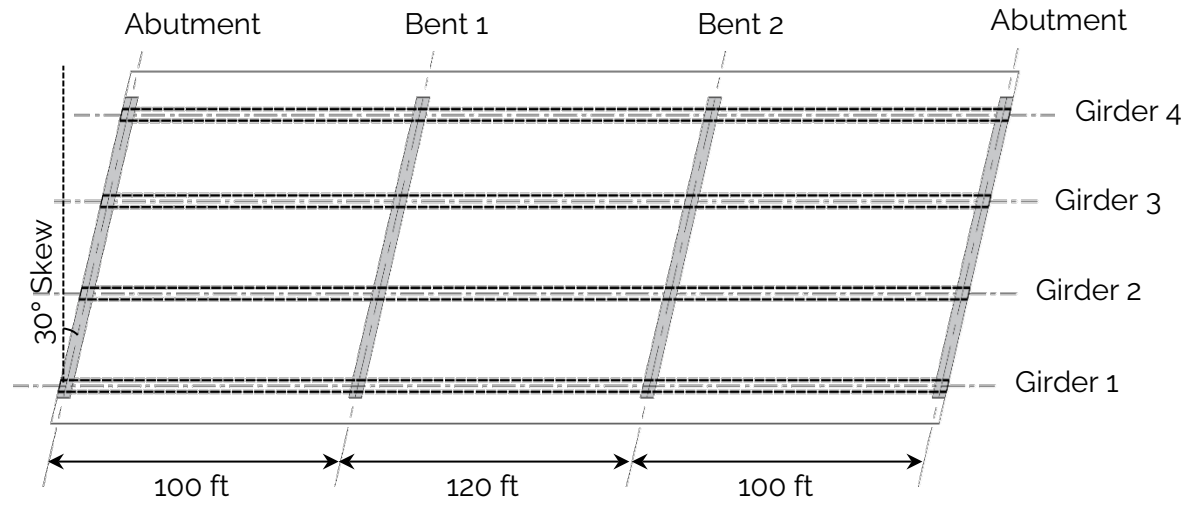

(a) Plan view

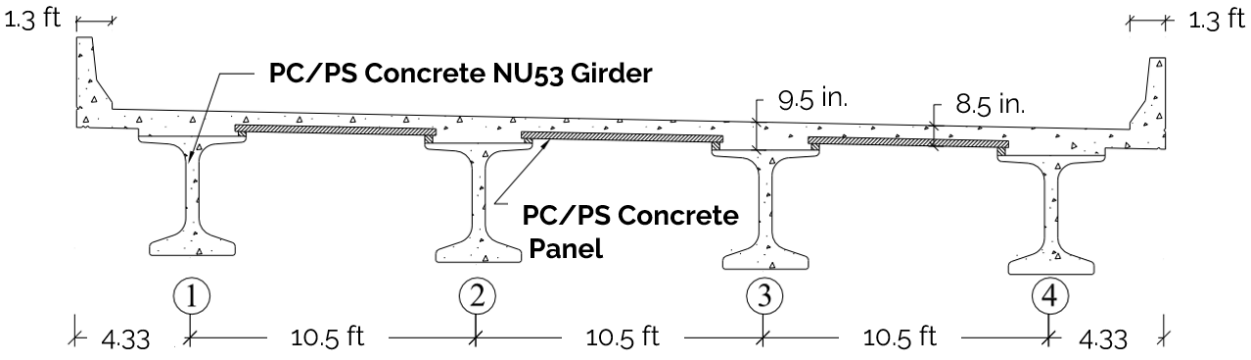

(b) Cross-section view

Figure 3-6. A7957 bridge details

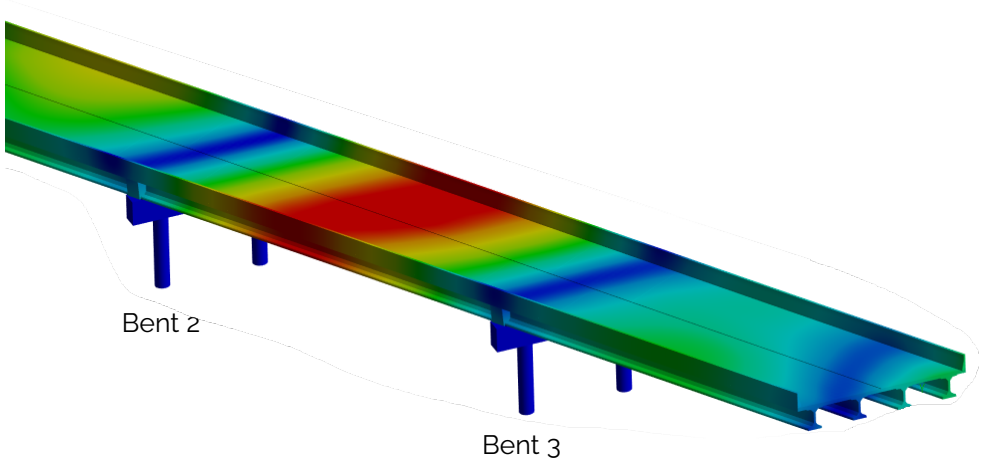

Figure 3-7. FE model for the validating Bridge A7957

A8697 Bridge

Bridge A8697 over Mussel Fork River, located in Keytesville, Missouri, was selected to represent non-skewed bridges for the purposes of modeling and analysis. The bridge has six spans with a total length of 561.5 ft, **Figure 3-8**. The bridge is supported by four NU43 precast girders and has five intermediate bents. A typical closed intermediate diaphragm with shear keys and dowel bars are used. The diaphragms measure 30.7 ft in length and 30 $in.$ in width, while the bent cap beams span 32 ft. Additionally, 18 #6 dowel bars, spaced at 10 $in.$ are used. The supporting columns of the bridge stand at a height of 6.6 ft with a diameter of 3 ft on top of 4 ft diameter 41 ft long shafts and 3.5 ft diameter 25 ft rock sockets.

The FE model was constructed utilizing consistent modeling criteria as discussed earlier. Concrete materials were characterized by a density of 145 lb/ft^3 and a Poisson's ratio of 0.2. Elastic moduli were assigned to various components: concrete columns, bent cap beams, diaphragms, and deck had a modulus of 4350 ksi, while girders were assigned an elastic modulus of 6525 ksi. Reinforcement elements were modeled with a density of 490 lb/ft^3 and an elastic modulus of 29,000 ksi. Grade 60 was used for steel rebar and dowel bars, while low-relaxation grade 270 was used for the prestressing strands. The FE model has shown a rotational stiffness (R_{kb}) of 277,237 $kip.ft/rad$. This rotational stiffness will serve as the base model for non-skewed bridges, and further parameters will be studied to investigate their influence on the rotational stiffness.

To validate the obtained rotational stiffness, a simplified analytical approach was used, employing cracked section analysis. To accurately represent the behavior of dowel bars, a slip model was considered based on a method developed by (Zhao & Sritharan, 2007). This approach integrates a hysteretic model for the reinforcing bar stress versus slip response into the analysis using a zero-length section element. It addresses strain penetration effects along fully anchored longitudinal reinforcing bars in concrete members, often overlooked in traditional analyses. The method effectively captures strain penetration effects, thus

overcoming the overestimation of rotational stiffness in fully bonded models that ignore strain penetration effects in concrete structure analyses. Based on this method, bond slip can be calculated using **Equation 5**. For 60 ksi steel and 4000 psi concrete, the slip at yield of a #6 bar was found to be 0.0188 $in.$ The distance from the center of the dowel bar to the edge of the joint filler in the diaphragm was 12.62 $in.$ Treating the interface of the diaphragm to bent cap as a cracked concrete section, the distance to the centroid of the compressive resultant (d-kd) is 10.7 $in.$ and the cracked moment of inertia is 8169 $in.^4$. Since the behavior remains within the linear zone, only the slope is of importance, therefore under an arbitrary moment of 600 $kip \cdot in.$ the steel stress using the cracked section analysis is 6.3 ksi. Using a linear relationship derived from the slip at yield (0.0188 $in.$), the slip at 6.3 ksi is 0.0019 $in.$ Dividing this value by the (d-kd) of 10.7 $in.$ a rotation of 0.00183 radians is obtained. The rotational stiffness (R_{kb}) was then determined as the ratio of the moment divided by the rotation, resulting in a value of 270,089 $kip.ft/rad$, which demonstrates good agreement with the FE model. Furthermore, it illustrates that most of the rotational restraint simply arises from the interface between the diaphragm and bent cap and that it behaves like a reinforced concrete section.

$$S_y = 0.1\left(\frac{d_b}{4000}\frac{F_y}{\sqrt{f'c}}(2\alpha+1)\right)^{\frac{1}{\alpha}}$$

Where:

S_y = the yield slip

d_b = the bar diameter in $inches$ = 0.75 $inches$

F_y = the yield strength of the bars = 60 ksi

$f'c$ = the compressive strength of concrete = 4,000 psi

α = the local bond-slip parameter = 0.4 in accordance with CEB-FIP Model Code 90 (FIB Task Group on Bond Models, 2000).

Equation 5. Bond-slip model (Zhao & Sritharan, 2007)

As part of this research project, experimental testing of Bridge A8697 was conducted to provide validation for the FE model, with detailed testing procedures and results to be discussed in **Chapter 4**. The FE model was constructed in accordance with the test setup, utilizing consistent loading procedures and data acquisition methods. In the validation process, a large-scale bridge model was constructed, incorporating two intermediate bents as shown in **Figure 3-9**. The model was then validated in terms of displacements at different locations and rotations, ensuring that the FE model closely matched the observed behavior during testing.

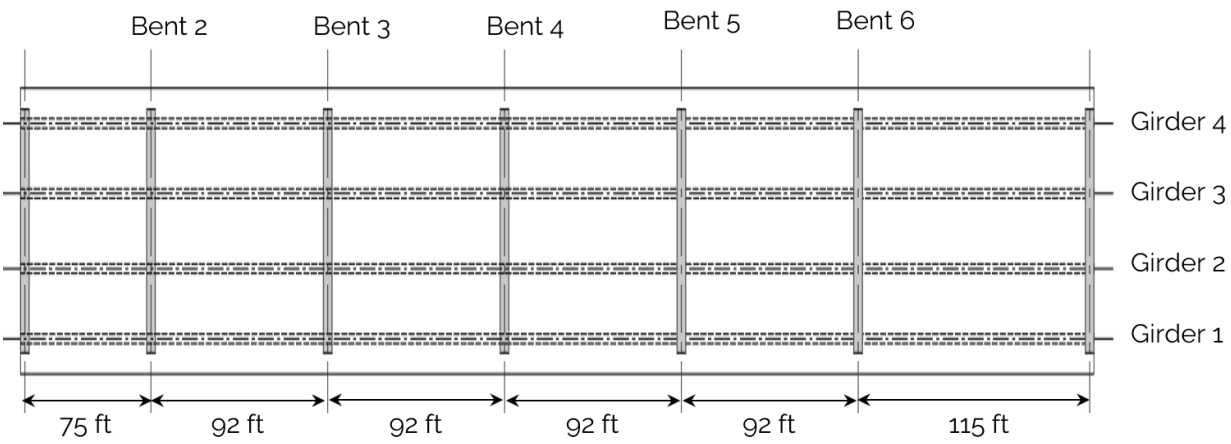

Figure 3-8. A8697 Bridge layout

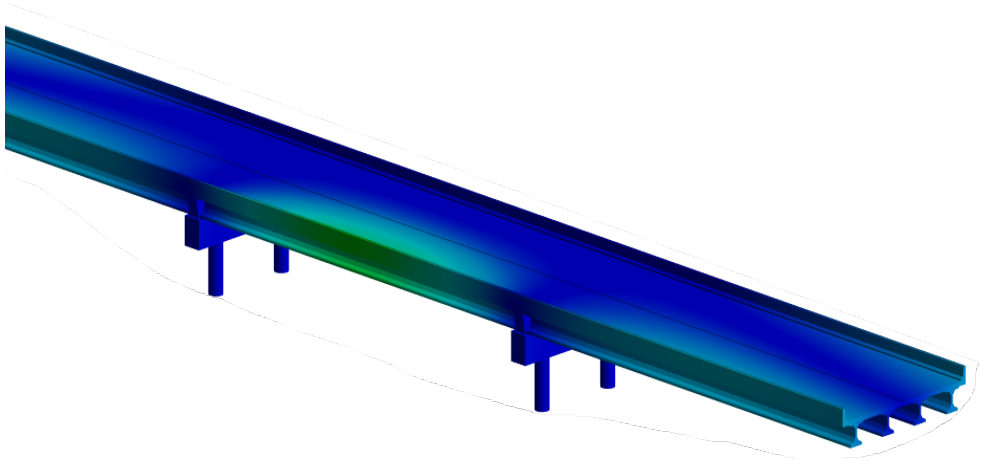

Figure 3-9. FE model for the validating Bridge A8697

A8279 Bridge

A third bridge, Bridge A8279, was included in this study to evaluate the use of H-piles. The bridge is a four-span box-girder section, with a box depth of 21 in. The diaphragms measure 27.67 ft in length and 34.5 in. in width, while the bent cap beams span 29 ft. Additionally, the bridge incorporates 10 #6 dowel bars, spaced at 12 in. The bridge has a skew angle of 30 degrees. H-piles (HP 14x73) were used as part of the bridge design, with a length of 23.5 ft.

The FE model was constructed utilizing consistent modeling criteria as discussed earlier, employing the same material properties as those found in the bridge plans. Concrete materials were characterized by a density of 145 lb/ft^3 and a Poisson's ratio of 0.2. Elastic moduli were assigned to various concrete components: bent cap beams, diaphragms, and deck had a modulus of 4350 ksi, while girders were assigned an elastic modulus of 6525 ksi. Steel H-piles were modeled with a density of 490 lb/ft^3 and an elastic modulus of 29,000 ksi.

The FE model has shown a rotational stiffness (R_{kb}) of 174,763 $kip.ft/rad$. This lower rotational stiffness, compared to Bridges A7957 and A8697, is primarily the result of the shorter length of the bent cap and the reduced number of dowel bars. This rotational stiffness would serve as one of the key models in our final analysis to represent the bridges with H-piles.

Summary

This chapter presents the finite element (FE) modeling approach used in this study to investigate the end restraint of intermediate bents in bridges. Bridge case studies were selected in collaboration with MoDOT's Bridge Division and Construction & Materials Division, ensuring representation of various configurations and design features. FE models were prepared for all bridges, including A7957, A8697, and A8279, using ANSYS workbench. The models were prepared using appropriate elements, and material properties were defined based on specifications outlined in bridge design documentation. The FE model was validated using Bridge A7957, previously tested by (Hernandez & Myers, 2016), and Bridge A8697, which underwent testing as part of this study. Following validation, a comprehensive parametric study was conducted to investigate the influence of various parameters on the rotational stiffness of intermediate bent connections. By applying horizontal displacement to a refined FE model of intermediate bents and analyzing resulting reactions, moment-rotation curves were constructed. The slope in the linear portion of these curves yields the rotational stiffness of the connections. Furthermore, rotational stiffness obtained was validated analytically using simplified cracked section analysis, with a slip model based on a method developed by (Zhao & Sritharan, 2007). Overall, the developed FE models demonstrated a robust approach to analyzing the rotational stiffness of intermediate bent connections in bridges.

Chapter 4. Experimental Testing

Bridge A8697 Rt. 24, located over the Mussel Fork River, was chosen to be tested as part of this study. The bridge was chosen due to its typical characteristics, representative of common bridges in Missouri, with short column height allowing easy access to the bottom of the girders, and having multiple uniform spans**, Figure 4-1**. The 3rd bent of the bridge was instrumented for the test. The testing involved loading the bridge with dump trucks positioned at various stations while recording the corresponding deflections and rotations using Digital Image Correlation (DIC) and Linear Variable Differential Transformers (LVDT). The results of the test were then used to validate the FE model.

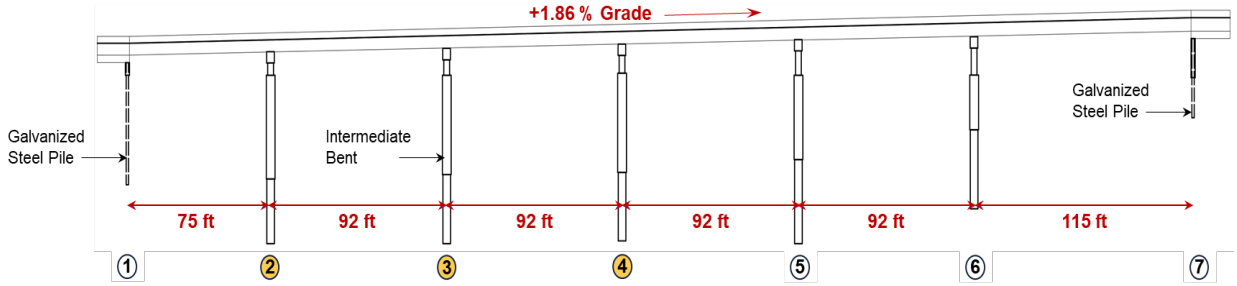

Figure 4-1. Elevation of bridge A8697, bent #3 was tested

Experimental Plan

To evaluate the degree of rotation at intermediate bent #3 under loading, loaded dump trucks were stationed between bents 3 and 4, as shown in **Figure 4-2**. Due to the fluctuations of DIC measurements with time, as discussed in **Chapter 2**, the testing was designed to quickly measure the unloaded and loaded movements. The bridge was closed to traffic for the duration of the testing window. Testing was conducted as follows: 1) a baseline recording using the LVDTs was made before the trucks were positioned on the bridge, 2) trucks were moved into position according to **Figure 4-3**, and the DIC system started recording, 3) trucks drove off the bridge. The total testing time was less than 2-3 minutes, and the testing was repeated three times to evaluate the reliability of the results.

Figure 4-2. Loading span 3-4 with dump trucks

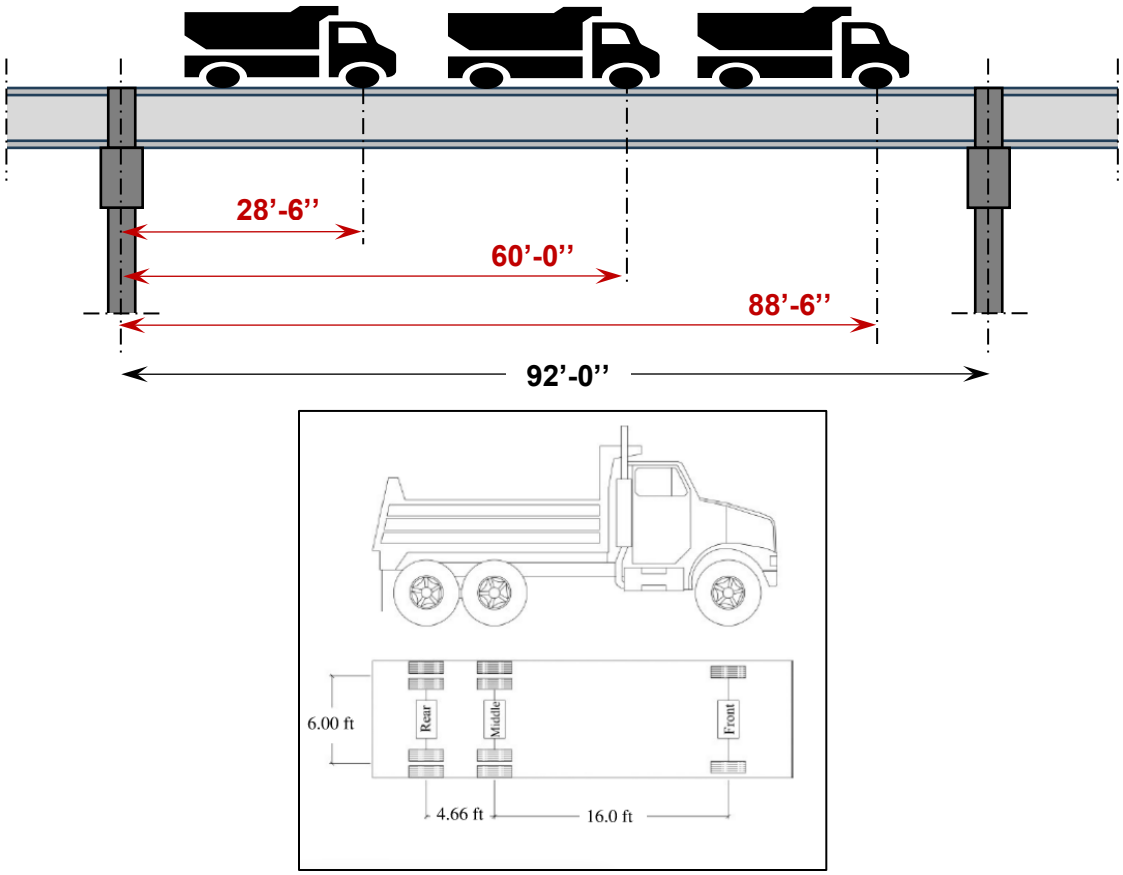

Figure 4-3. a) Trucks positions on span 3-4, b) Typical MoDOT H20 dump truck

Instrumentation consisted of the DIC system and four LVDTs. The LVDTs (BDI test model LVDT-01-010 with ±1.0 $in.$ range) were positioned as follows (**Figure 4-4**): 1) near the midspan of the loaded girder (the LVDT could not be placed at midspan because the supporting tripod could not

extend high enough, so the position was moved to 6 ft closer to bent #3), 2) On the loaded side girder, located 5 $in.$ transversely and longitudinally from the girder flange corner, 3) On the bent cap, located 5 $in.$ from the bent cap corner, and 4) On the unloaded side girder, positioned 5 $in.$ from the flange corner. Metal plates were affixed to the bottom of the concrete surfaces to ensure accurate measurement.

A system of 3 digital cameras was used in the DIC system. The digital cameras were attached to a grooved metal mounting bar, that allowed all three cameras to be quickly placed level and perfectly perpendicular to the target. The cameras were placed at a distance of 25 ft from the intermediate bent. The distance between the cameras and the target was chosen such that a small stereo angle or angle formed from the distance between the cameras and the target (~23 degrees) was obtained, for better in-plane accuracy (Dantec Dynamics, 2018). Random speckle patterns with 1.5 mm (0.06 in.) speckles (sufficiently greater than the minimum) were printed onto a sticky paper attached to the bridge to create high-contrast targets. These patterns were generated using a speckle pattern generator to create a target with 50% white and 50% black areas with 1.5 mm speckle sizes. These patterns were attached to the top and leftmost corner of the bent cap, bottom leftmost corner of the diaphragm, and rightmost edge of the girder flange, as shown in **Figure 4-5**. All three target patterns were in direct sunlight on the day of field testing. The weather conditions during the testing period had very little to no cloud cover, which meets ideal illumination conditions. Furthermore, the targets were placed closest to the adjacent span from the one being loaded during the test, to capture the difference in movements between the diaphragm and bent cap, as concluded using the FE model. The FE model indicated that the difference would be most pronounced at the opposite corner.

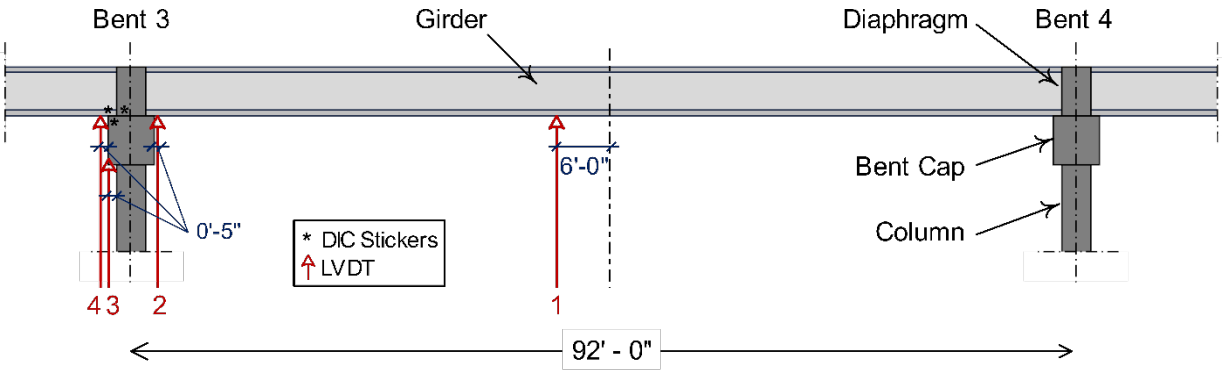

Figure 4-4. LVDT locations

Figure 4-5. DIC camera setup and target locations

Experimental Results

DIC Results

The images captured during the three field tests were analyzed in the software Istra-4D by Dantec Dynamics. Three separate analyses were completed on each test to isolate the

movement of the bent cap, diaphragm, and girder individually. **Figure 4-6** shows a snapshot of the analysis of the DIC data in the Istra-4D software for the bent cap during test 1. An area of approximately 4 $in.$ by 4 $in.$ was chosen on the speckle pattern, and the computed DIC displacements were averaged over this area to determine a single displacement history versus time. The displacement data was then passed through a low-pass Butterworth Filter to remove the high-frequency noise from the actual data. For the DIC data, the average displacement was taken as the difference between the average position while the trucks were on the span subtracted from the average position once the trucks were removed from the span, as shown in **Figure 4-7**.

The DIC system provides full-field displacement measurements and thus x and y (in-plane) displacements are provided. Istra-4D can produce an image overlay that indicates the direction of displacement over the captured image. For the bent cap, diaphragm, and girder, the overlay indicates that as the trucks are removed from the span, each component moves upwards and to the right (**Figure 4-6**). This indicates that the loading of the trucks on the span causes each component to move downward and to the left. **Table 4-1** presents the obtained DIC displacement results. In this table, positive values indicate movement upward and to the right during unloading.

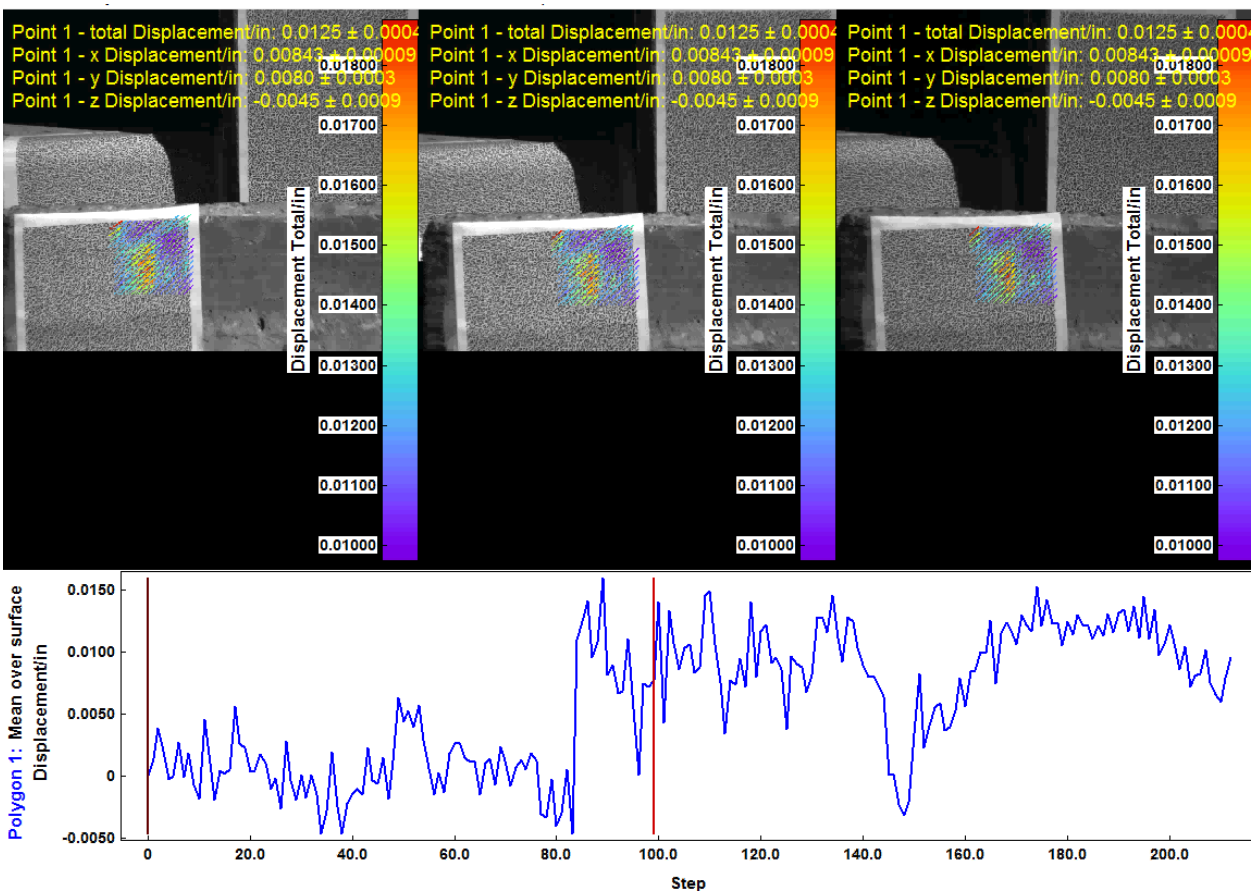

Figure 4-6. Analysis of DIC data in Istra4D software

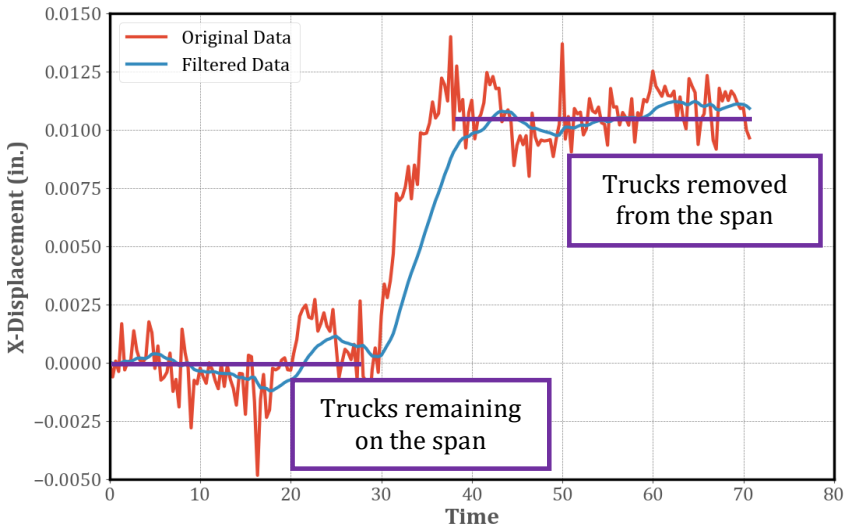

Figure 4-7. Filtering of data and determination of displacement for the bent cap beam (test 1)

All results contained significant levels of noise that needed to be removed using a Butterworth Filter. Notably, the vertical direction displacement results contained more noise than the horizontal direction displacement results for all tests and components. This can be attributed to the stability of the camera and tripod setup utilized during the experiments. As shown in **Figure 4-5**, the grooved metal mounting bar provides rigidity against any movements parallel to its length. However, transverse to the length of the bar, stability relies solely on the tripod legs. Factors such as breeze, ground shifting, or inadvertent human contact with the camera setup could shift the camera position. Given the scaling factor used in the analysis, even a minor shift in the camera view by a few pixels can cause the software to interpret a significant change in displacement of nearly 1 *mm* (0.04 in.). Thus, the vertical displacements have greater levels of noise than the horizontal displacements. The vertical displacements from Test 2 contained such high levels of noise that the change in displacement caused by the trucks was fully obscured, thus they were omitted from discussion.

The overall x and y displacement results for the bent cap, diaphragm, and girder are given in **Table 4-1** while complete data is available in the Appendix. The horizontal displacements were very similar between all three tests. For the bent cap, diaphragm, and girder, all three tests gave resulting displacements on the order of 0.01 $in.$, indicating that each component likely moved to the left under loading by the same amount. The vertical displacements for Test 3, however, are nearly 0.015 $in.$ greater than those obtained in Test 1. Given the scaling factor, this translates to a shift of only 1.4 pixels in the camera field-of-view. This drifting behavior can be attributed to a shift in the camera position while the image capture was occurring. Due to this drift, confidence can only be had in the y-displacement results of Test 1.

Table 4-1. Overall DIC x and y displacements
(+ indicates downward and to the left movements under loading)

X-Displacements (in.)			
	Bent Cap	**Diaphragm**	**Girder**
Test 1	+0.012	+0.0096	+0.0087
Test 2	+0.013	+0.012	+0.011
Test 3	+0.014	+0.013	+0.0099

Y-Displacements (in.)			
	Bent Cap	**Diaphragm**	**Girder**
Test 1	+0.012	+0.0087	+0.0072
Test 2	-	-	-
Test 3	+0.026	+0.025	+0.023

Rotations were calculated for the intermediate bent components using the DIC results. For the bent cap, diaphragm, and girder analyses, two (2) point gages were created as far apart as the image allowed. Tracking the x displacements (due to higher accuracy of the x displacements) of the two points allowed for the calculation of the angle of rotation (θ) using **Equation 6,** as can be seen in **Figure 4-8**. The resulting rotations are shown in **Table 4-2**. The rotations of the bent cap were ten times less than the rotations of the diaphragm and the girder, indicating that there was a significant difference in the rotation of the girder and diaphragm compared to the bent cap. While the girder shows slightly higher rotations compared to the diaphragm, both were within the same order of magnitude of $1\ x\ 10^{-4}$ radians. The diaphragm is cast around the girder ends so it reasonable to see that they move together as a unit. These results indicate that the primary rotation occurs at the joint connection between the diaphragm and bent cap.

$$\theta = \tan^{-1}\frac{dx(B) - dx(A)}{known\ length}$$

Where:

θ = is the angle of rotation

$dx(A)$ = is the horizontal displacement of point A

$dx(B)$ = is the horizontal displacement of point B

Equation 6. Calculating the angle of rotation using DIC data

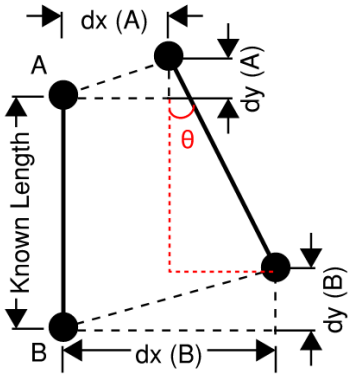

Figure 4-8. Calculation of rotations using DIC displacement data

Table 4-2. Rotations of bent cap, diaphragm, and girder measured by DIC

Relative Rotations (radians)			
	Bent Cap	**Diaphragm**	**Girder**
Test 1	0.000033	0.000275	0.000400
Test 2	0.000033	0.000125	0.000800
Test 3	0.000067	0.000250	0.000600

LVDT Results

LVDTs were also used to record the vertical movements of intermediate bent components over time. The reduced computational needs of LVDT data allowed for continuous readings, including periods before, during, and after the presence of trucks on the bridge. The LVDT data were also passed through a low-pass Butterworth Filter to reduce the noise. For each of the three tests, time windows of the different loading stages were defined as A) before the trucks were loaded onto the span, B) while the trucks were stationary on the span, and C) after the trucks were removed from the span. Consequently, the displacement was calculated between points A and B and points B and C. **Table 4-3** gives the average results from the loading and unloading of the bridge for each of the three tests. Positive values indicate downward movements.

Figure 4-9, **Figure 4-10**, and **Figure 4-11** present a comprehensive analysis of displacement versus time curves obtained using the LVDT data. The LVDT movements measured across the three tests were very consistent indicating accuracy in the results, although the accuracy of the LVDT was only ±0.001 in. The results also show a prominent downward movement in the loaded side girder during loading, that is significantly larger than the unloaded side girder (which slightly moved upward), indicating overall rotation in the joint. Furthermore, as expected, bent cap displacements were considerably smaller than those obtained on the loaded side of the girder.

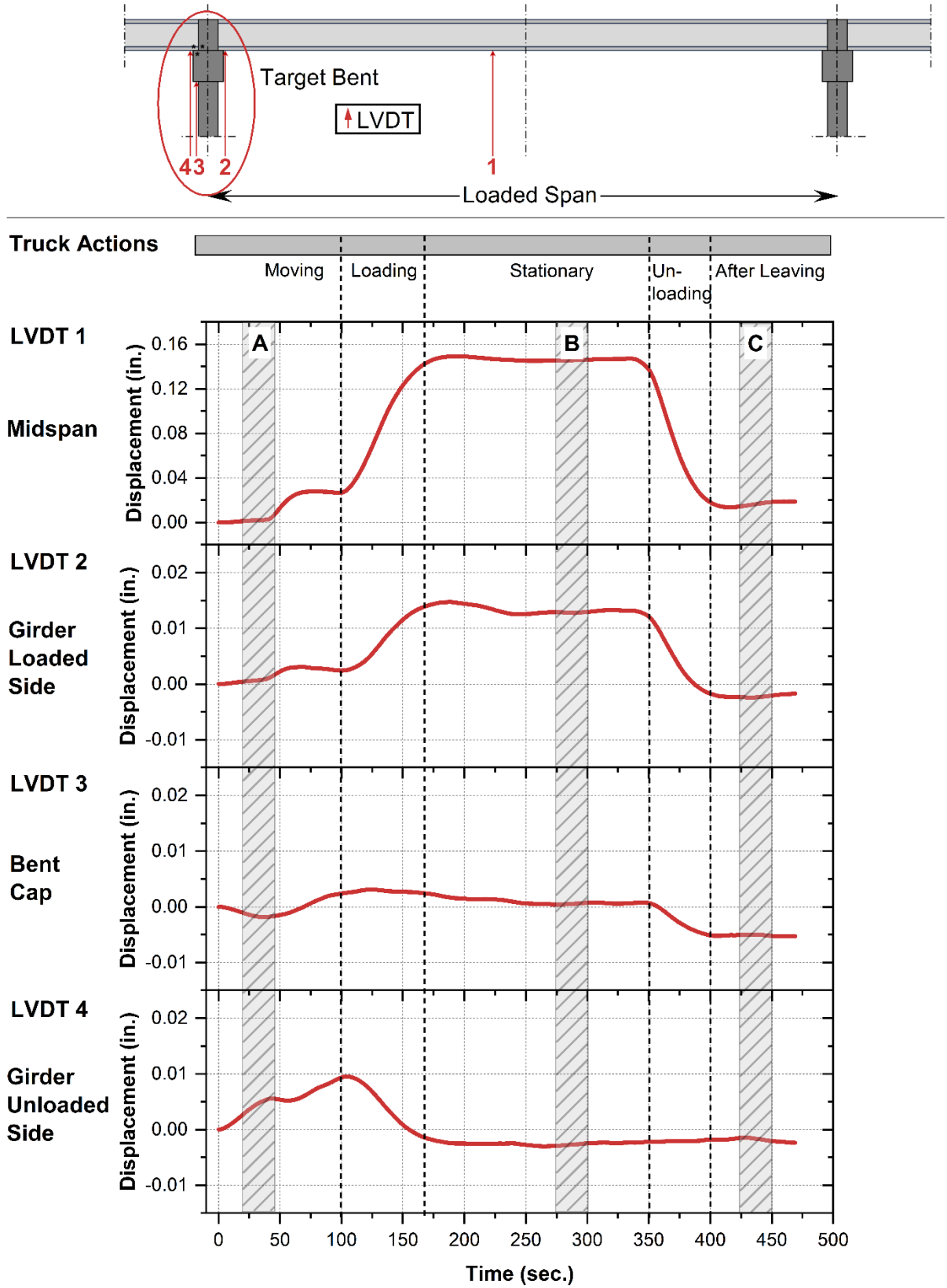

Figure 4-9. Example LVDT readings during testing for test run #1

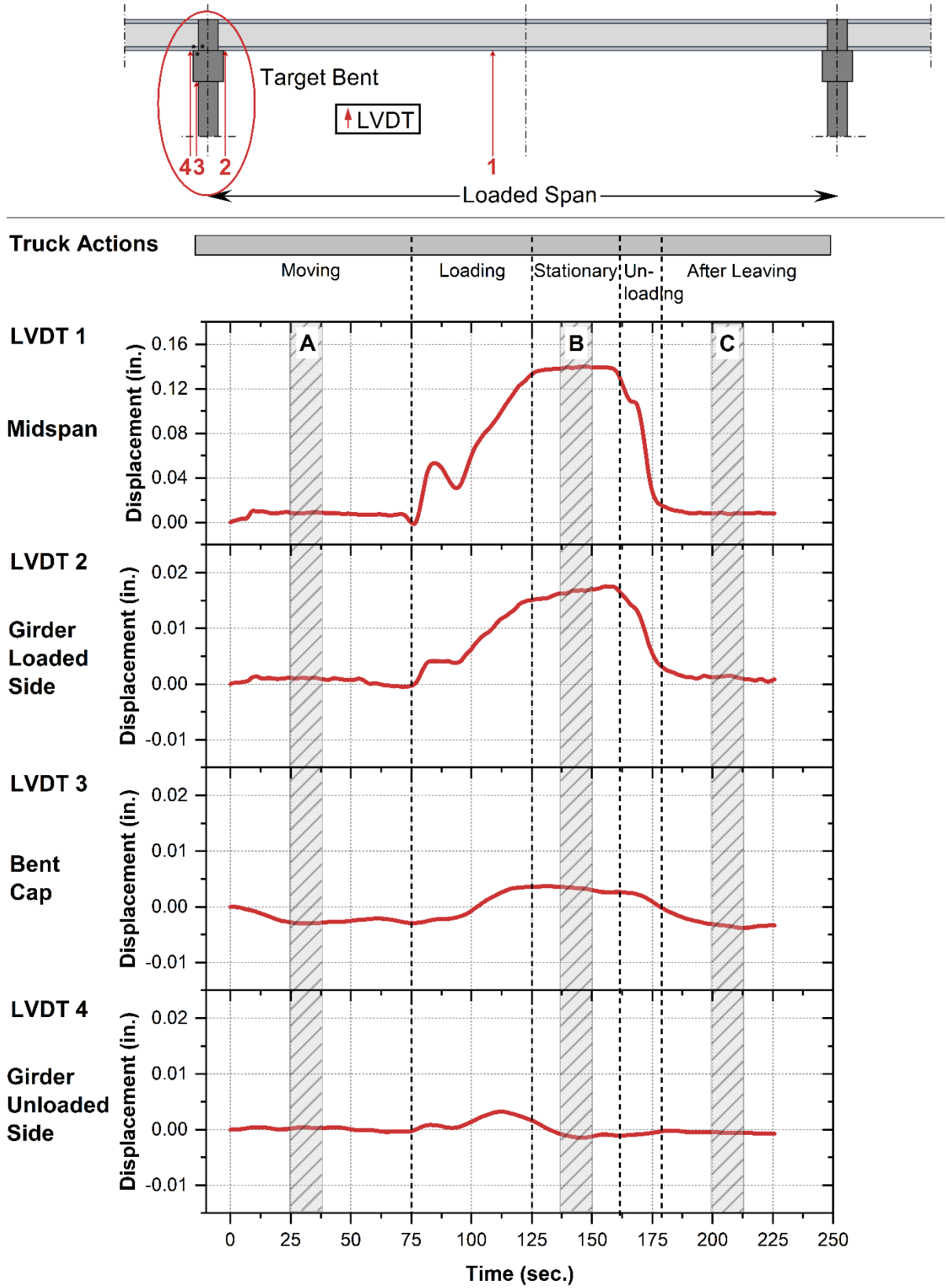

Figure 4-10. Example LVDT readings during testing for test run #2

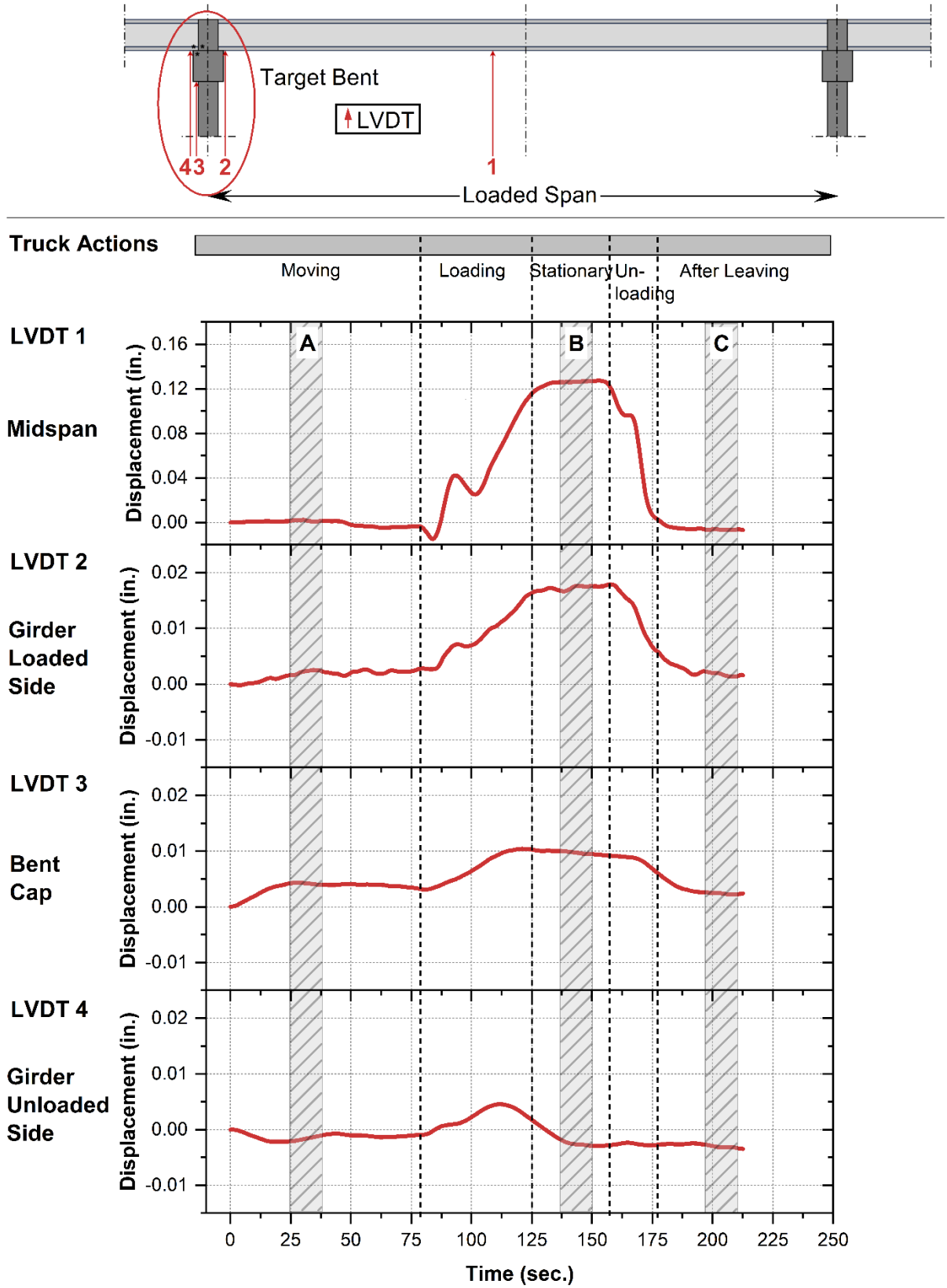

Figure 4-11. Example LVDT readings during testing for test run #3

Table 4-3. Average LVDT results (in.)
(+ indicates downward movements under loading)

Test	LVDT 1 Midspan	LVDT 2 Girder Loaded Side	LVDT 3 Bent Cap	LVDT 4 Girder Unloaded Side
1	+0.138	+0.014	+0.006	-0.001
2	+0.131	+0.016	+0.006	-0.001
3	+0.129	+0.016	+0.007	0.000
Average	+0.1326	+0.0153	+0.0068	-0.0001

Comparison of FE Predictions, with LVDT and DIC Data

Comparison of the DIC data versus the finite element model (FEM) prediction at the same locations as the DIC measurements under the loading applied during the testing is given in **Table 4-4**. While there is a significant difference in the vertical displacement of the bent cap, the vertical displacements of the diaphragm and unloaded side girder are very close to the FEM prediction. The horizontal displacements are more accurate and show that the FEM model was able to reasonably predict the movements of the bridge under testing.

Table 4-4. DIC vs FEM predictions

Vertical Displacement

	Bent Cap	Diaphragm	Girder Unloaded Side
DIC (in.)	0.012	0.009	0.007
FE (in.)	0.006	0.005	0.007
Absolute Difference	0.004975	0.0037	0.0002

Horizontal Displacement

	Bent Cap	Diaphragm	Girder Unloaded Side
DIC (in.)	0.013	0.012	0.009
FE (in.)	0.014	0.019	0.007
Absolute Difference	0.001	0.007	0.002

A comparison of the vertical displacements of the LVDTs versus the FEM is given in **Table 4-5**. While the FEM prediction of the midspan displacement shows the greatest difference from the

experiment, the difficulty of obtaining this measurement on a 14 ft extended tripod may have impacted the accuracy of the results. The displacements of the loaded side girder and bent cap show good agreement with the FEM model. There is some discrepancy between the DIC and LVDT displacements in the bent cap and unloaded side girder; however, there was difficulty in obtaining accurate vertical displacements from the DIC.

Table 4-5. Comparison of vertical LVDT, DIC, and FEM displacements

Test	Midspan	Girder Loaded Side	Bent Cap	Girder Unloaded Side
LVDT (in.)	0.133	0.015	0.006	0.0008
DIC (in.)	N/A	N/A	0.012	0.007
FE (in.)	0.202	0.019	0.006	0.007
LVDT vs FE	0.069	0.004	0.000	0.006

The rotation data from the DIC system shows the best agreement with the FEM model, **Table 4-6** and **Figure 4-12**. The predicted rotations in the bent cap, diaphragm, and unloaded side girder all agreed well with the FEM model with the error in the bent cap and unloaded side girder being only 13% and 11%. The diaphragm showed more error at 75%, but given the difficulty in obtaining the very small movements, it is still reasonable. Given that rotational restraint, and thus rotational movement, is the most important parameter for this research, the accuracy of the rotations demonstrates the accuracy of the FEM model for the estimation of the rotational restraint at the top of the column.

Table 4-6. Comparison of DIC and FEM rotations

Test	Bent Cap	Diaphragm	Girder Unloaded Side
DIC (rad)	0.000033	0.000263	0.00050
FE (rad)	0.000029	0.000445	0.00045
Absolute Difference	4.00E-06	1.82E-04	5.00E-05

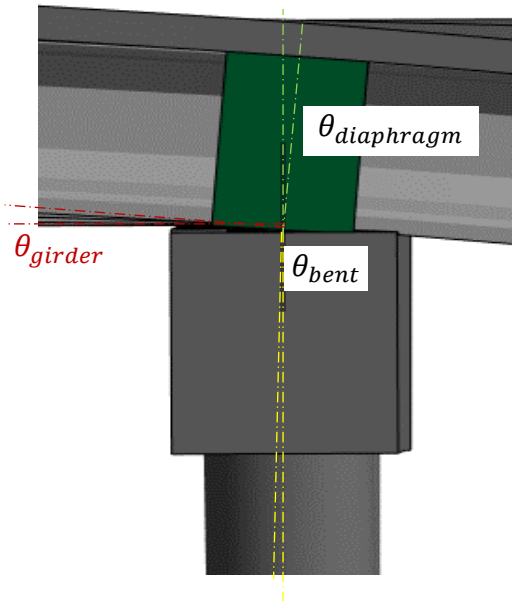

Figure 4-12. Rotations in intermediate bent

Dowel Bar Development

One of the assumptions in the FE model was that the dowel bars were fully bonded to the concrete. However, the dowel bars are typically only inserted at 12 to 15 in. which is less than their full development length. In the FE model for the A8697 bridge the stress in the bars under the full loading was 17.7 ksi, much less than the yield stress and able to be developed with the design embedment length. If designers chose to use the reduced k-factors in this study they should either check the stress in the dowel bars under design loading, or provide sufficient development length for the bars.

Summary

Experimental testing was conducted on bridge A8697 via loaded dump trucks. The movements of the bridge were recorded via DIC and LVDTs. The DIC data showed good accuracy in the horizontal direction but was less accurate in the vertical direction due to possible movements in the camera. The DIC rotation data showed that the girder and diaphragm rotated together with about 10 times more rotation than the bent cap supporting the FE model showing most of the rotational flexibility due to the bent cap to diaphragm connection. The LVDT data was consistent across all three test runs and generally matched the FE model predictions for the bent cap and loaded side girder deflections. However, both the FE and DIC measurements were very small and barely out of the noise of the devices.

Chapter 5. Parametric Analysis

With the validated FE model, a parametric analysis can be conducted to determine the sources and relative impacts of parameters affecting the rotational restraint of the intermediate bent. The first step was to identify the key parameters that may impact the rotational restraint of the connection. From examining the bridge plans the research team selected the most influential parameters to be: column length and stiffness, girder length and stiffness, girder depth, connection interface, concrete stiffness, dowel bar area, diaphragm width, and skew angle. The following presents a detailed analysis of each of the parameters. The detailed analyses were based on the FE model for bridge A8697, in which changes in the bridge characteristics (such as the number of dowel bars) were changed one at a time for a parametric analysis. The chapter concludes with an optimized equation to predict the rotational stiffness of the connection.

Column Length and Stiffness

As presented in **Chapter 2**, the column length and stiffness directly affect the k-factor and can be accounted for in the equation for the k-factor. In short, as the column becomes longer or less stiff, the amount of rotational restraint needed to make the connection behave as fixed becomes less. As the column length and stiffness are already accounted for in the k-factor it does not need to be considered as a parameter in the determination of the rotational restraint at the top of the column.

Girder Length and Stiffness

The girder length and stiffness can affect the rotational restraint at the top of the column. In basic steel frames, such as in buildings, the joint itself is considered to be stiff (rotationally rigid) and the flexibility of the connecting beams determines the k-factor for the column. In the case of the intermediate bents, the joint is not stiff and the rotational restraint at the top of the column would be the combination of the rotational restraint of the girders and the joint as shown in **Figure 5-1**. However, the approximate rotational restraint provided by one 92 ft long NU43 girder would be ~608,000 $kip \cdot ft/rad$ whereas the restraint determined in joint from bridge A8697 was only ~300,000 $kip \cdot ft/rad$ (see **Chapter 3**). Therefore, with 8 total girders framing the joint, the rotational stiffness of the girders is so much greater than the stiffness of the joint, that almost all the rotational flexibility is accounted for in the joint. Therefore, the girder length and stiffness were determined to not be significant factors in the rotational restraint at the top of the column.

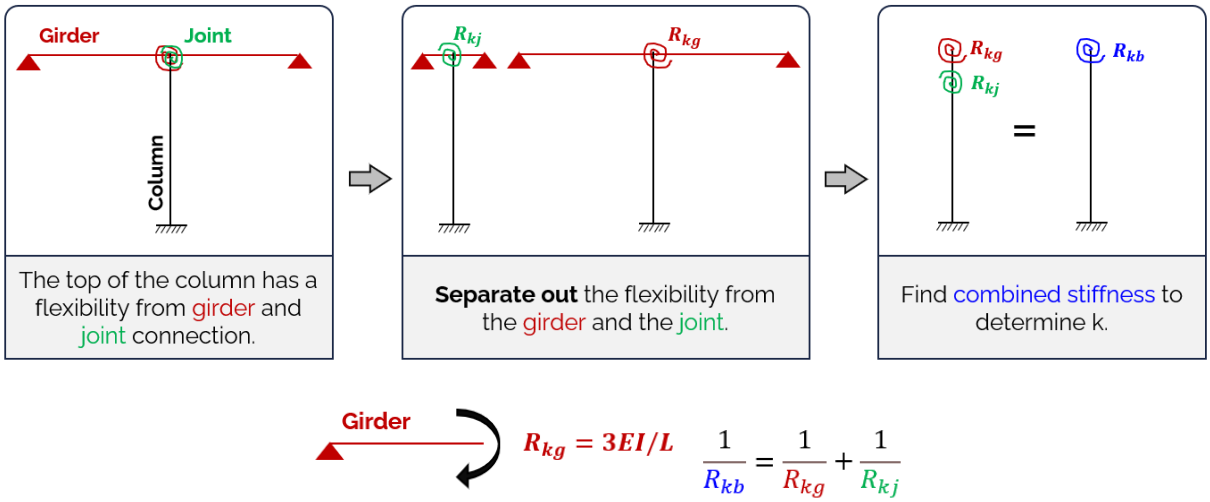

Figure 5-1. Combination of girder and joint rotational restraint

Girder Depth

In addition to girder length and stiffness, the effect of the girder depth was also analyzed in the FE models. Three models were run with a girder depth of 35 $in.$ (NU 35), 43 $in.$ (NU 43) and 70 $in.$ (NU 70). The results shown in **Figure 5-2** show that the girder depth does not affect the rotational restraint of the joint. This is expected because most of the movement in the joint occurs between the diaphragm to bent cap connection and the girders and diaphragm behave together rigidly. Thus, the depth of the girder is not a significant parameter in the rotational restraint at the top of the column.

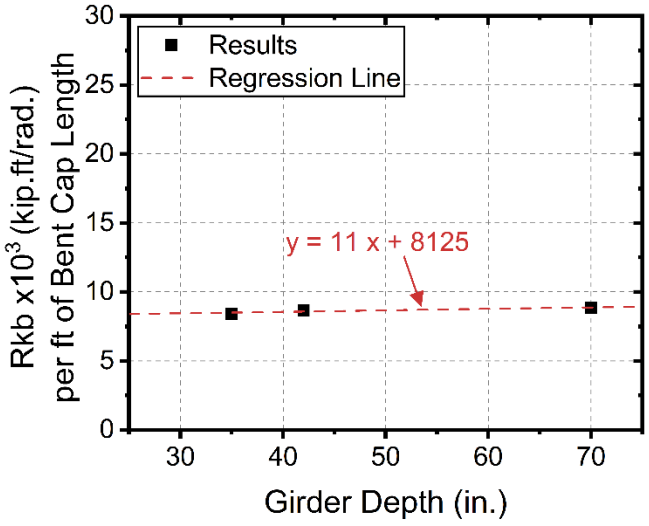

Figure 5-2. Effect of girder depth on rotational restraint

Bent Cap Length

A major variable in the determination of rotational restraint of the joint is the length of the diaphragm. As the length becomes longer, the joint will become stiffer, just as how a wider reinforced concrete beam is stiffer as the moment of inertia increases due to b. Therefore, the simplified equation to predict rotational restraint presented at the end of this chapter is the restraint per ft length of the bent cap. The bent cap length is used instead of the diaphragm length because it is more easily read from the plans and is generally, similar to the diaphragm length. If there is a situation where this is not the case, designers should use the diaphragm length.

Connection Interface

Details of the connection interface can play a significant role in the rotational restraint of the joint. To examine the potential impact of some of the standard details, an evaluation of the effect of the shear key and connection interface was made. As seen in **Figure 5-3**, standard MoDOT details include the use of shear keys and a layer of roofing felt to act as a bond breaker between the cast-in-place diaphragm and bent cap top. A FE model was created to examine the impact of the presence of the shear keys on rotational restraint, **Figure 5-4**, and found that the shear keys do influence the rotational restraint with the removal of the shear key reducing the restraint by about 35%. In addition, the layer of roofing felt between the diaphragm and bent cap is very significant. The FE model considered a fully bonded connection between the diaphragm and the bent cap and the rotational restraint increased by about 5 times. Although these details do have a significant effect on the rotational restraint, as they are part of the standard details, they are not considered in the simplified equation to predict rotational restraint presented at the end of this chapter. If MoDOT changes these details, then the equation may need to be updated as well.

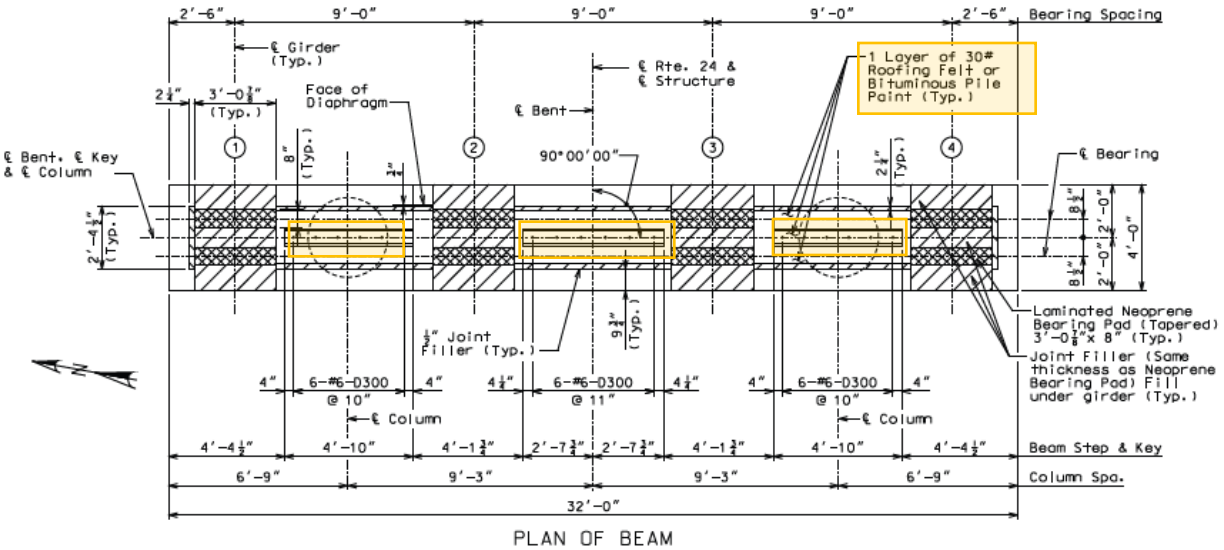

Figure 5-3. Typical connection highlighting shear keys and roofing felt layer (Bridge A8697)

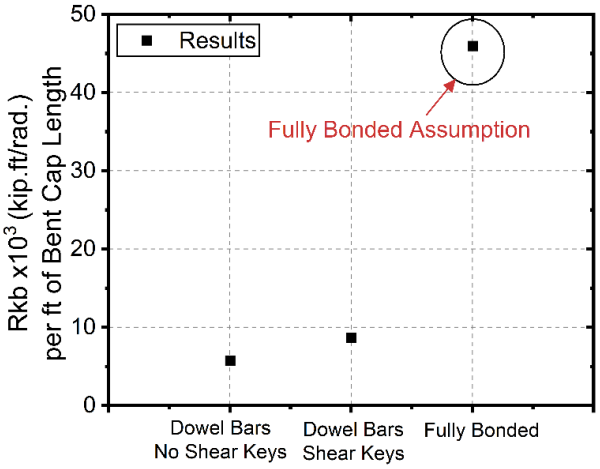

Figure 5-4. Effect of shear keys and bonding on rotational restraint

Dowel Bar Area

As described in **Chapters 2** and **3**, the connection between the diaphragm and bent cap top is critical in the rotational restraint at the top of the column. The dowel bars provide an important connection between these two interfaces. As shown in **Chapter 3**, the connection can be idealized with sectional analysis with the dowel bars providing the important tensile strength in the rotation. Therefore, an analysis was conducted to determine the impact of the dowel bar size and number. A FE model was created with different dowel bar diameters of 0.2 $in.$, 0.75 $in.$ and 2 $in.$, **Figure 5-5**. The model assumed that the bars were fully bonded to the concrete. Although the upper and lower diameters are out of the bounds of typical reinforcement, they help to establish the linear trend in the results. In addition, an increase in the number of dowel bars from 18 #6 bars to 33 bars was considered, **Figure 5-5**. These results were combined into a relationship between the total dowel bar area and the rotational restraint, as shown in **Figure 5-6**, which shows a slope of about 311 $kip \cdot ft/rad$ per $in.^2$ of total dowel bars. This slope value would need to be included in the final simplified equation to predict the rotational restraint.

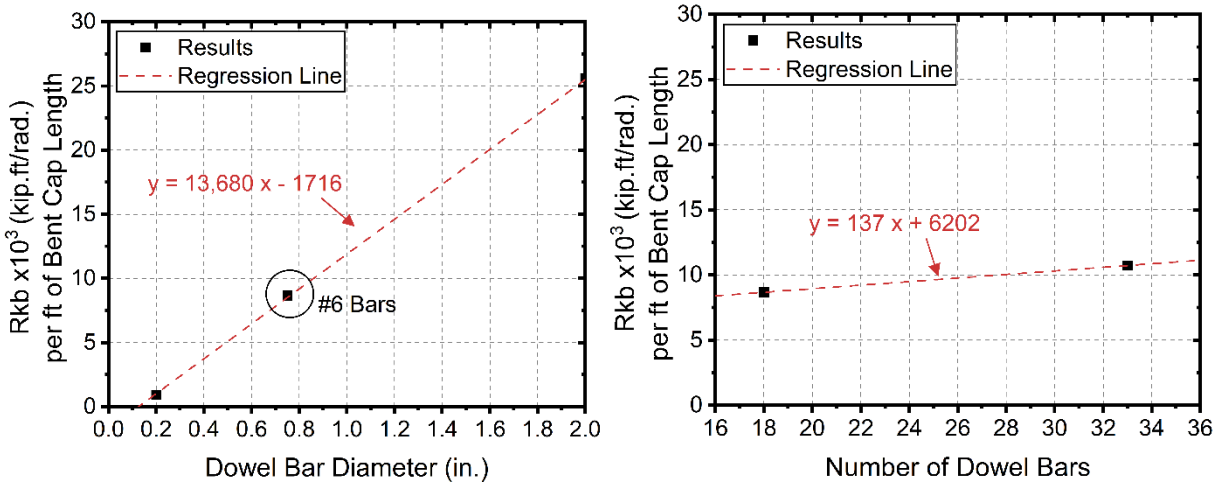

Figure 5-5. Effect of dowel bar size and number on rotational restraint

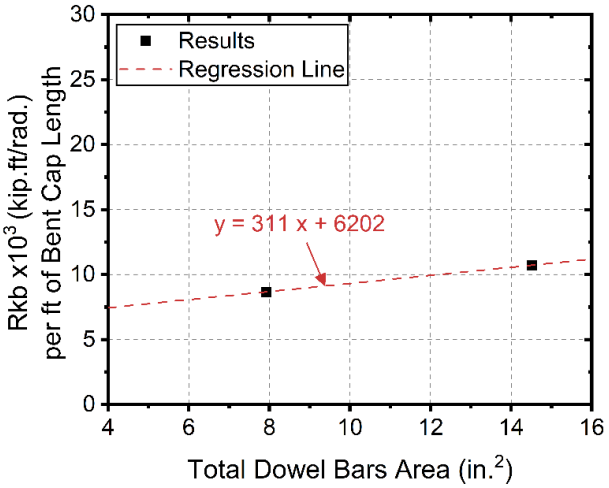

Figure 5-6. Effect of total dowel bar area on rotational restraint

Concrete Stiffness

The stiffness of the concrete was also analyzed in the parametric study. As the connection between the diaphragm and the bent cap relies on the tensile force developed in the dowel bars and the compressive force in the concrete, the stiffness of the concrete is directly related to the stiffness of the connection. In addition to the standard model of the A8697 bridge with a modulus of 4350 ksi, an additional model with a concrete modulus of 2176 ksi (which would correspond to poor concrete) was run. The results (**Figure 5-7**) show a 25% reduction in the rotational stiffness with the much lower E value. For a typical estimated concrete modulus of 3605 ksi for a 4000 psi concrete (using ACI 318 19.2.2) the expected rotational stiffness would be 90% of the values presented. As the modulus of concrete can be highly variable, even with the same design strength, it is suggested that the calculated rotational restraint be reduced to account for possible lower values of modulus. A 2003 report by (Nowak & Szerszen, 2003) gave the concrete compressive strength of 4000 psi a bias of 1.226 and a COV of 0.1. Meaning that most concrete at a design strength of 4000 psi has a higher strength.

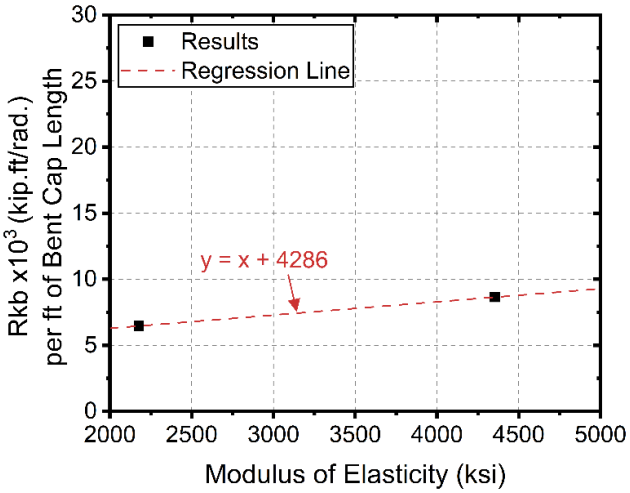

Figure 5-7. Effect of concrete modulus on rotational restraint

Diaphragm Width

The width of the diaphragm directly affects the rotational restraint at the top of the column. As discussed in **Chapter 3**, the connection between the diaphragm and the bent cap essentially acts as a moment couple (like in reinforced concrete) in which the dowel bars provide the tensile component and the concrete the compressive component. The width of the diaphragm influences the moment arm length and thus directly impacts the rotational resistance. A FE model based on the A8697 bridge was created with an original diaphragm width of 30 in. The model was then modified, with the diaphragm width increasing to 42 in. The results shown in **Figure 5-8**, demonstrate that the diaphragm width has a strong influence on rotational restraint, as expected, with a slope of 597 ($kip \cdot ft/rad$ per in. width diaphragm). This slope value would need to be included in the final simplified equation to predict the rotational restraint.

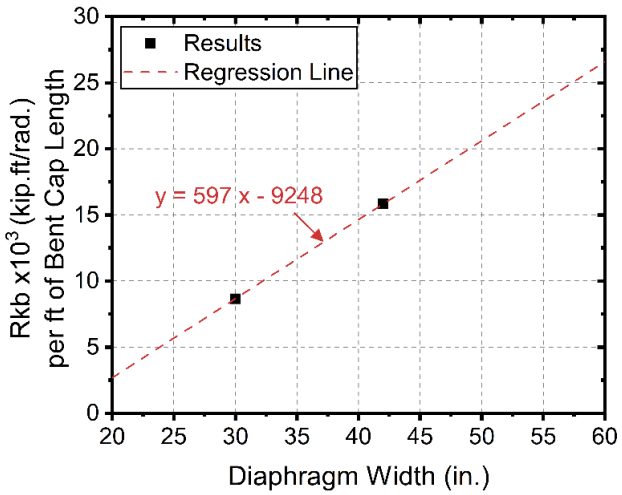

Figure 5-8. Effect of diaphragm width on rotational restraint

Skew

The skew of the bridge also impacts the degree of rotational restraint. One major source of this impact is that as the bridge is skewed the width of the diaphragm needs to increase. To examine the impact of skew, new drawings for the A8697 bridge were created assuming a skew of 22.5 degrees and 45 degrees (**Figure 5-9**). Due to the skew, the diaphragm width of the 22.5 degrees skew increased from 30 in. to 40.5 in. and the bent cap length increased to from 32 ft to 35 ft. Similarly, for the 45 degrees skew the diaphragm width increased to 46.5 in. and the bent cap length to 44 ft. The results of the FE models are shown in Error! Reference source not found.. However, as the skew and the diaphragm width are linked (they are not independent variables) the slope in **Figure 5-10** cannot be used directly in the simplified equation for rotational restraint. To isolate the effect of the skew, the influence of the diaphragm width and dowel bar area was subtracted from the rotational restraint using the slope values found earlier. The results, **Figure 5-11** (which includes bridges A7957 and A8279), show that once the

other factors are removed, skew has a negative effect on the rotational restraint with a slope of about $-195\ kip \cdot ft/rad$ per degree skew. The negative slope is likely caused by the fact that as the girders are skewed the effective length of the diaphragm is reduced resulting in less

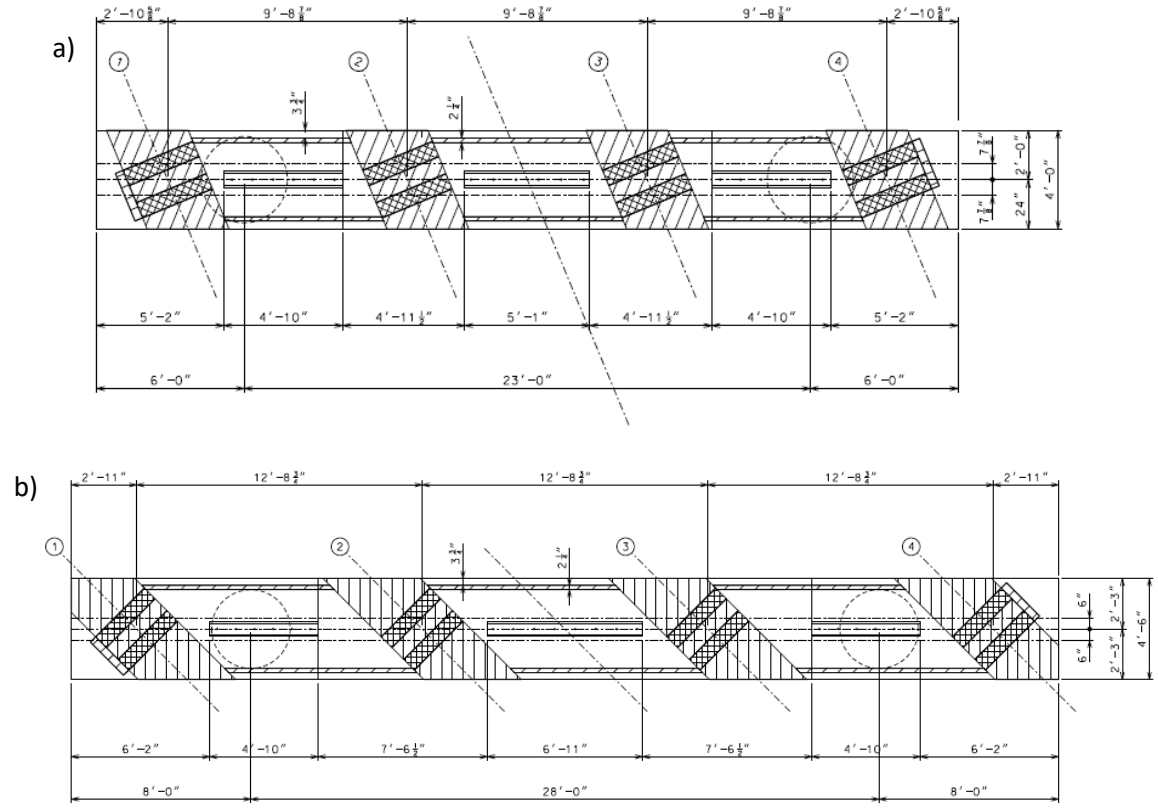

compressive resultant in the moment couple.

Figure 5-9. Skewed versions of A8697 with a) 22.5 degrees skew and b) 45 degrees skew

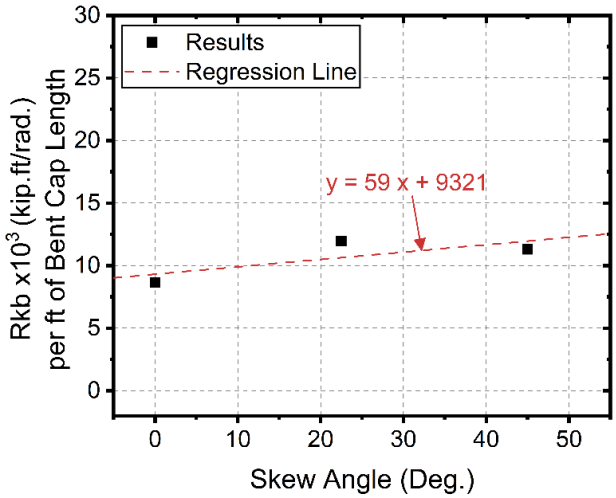

Figure 5-10. Effect of skew on rotational restraint (effect of diaphragm width and dowel bar are included)

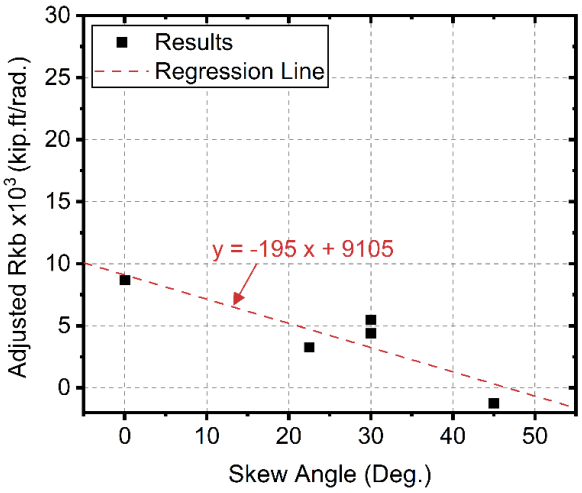

Figure 5-11. Effect of skew on rotational restraint (effect of diaphragm width and dowel bar area subtracted)

Summary of Parameters

A parametric analysis was performed to determine the influence of several key parameters on the rotational restraint at the top of intermediate bent columns. The results are summarized in **Table 5-1**. The parameters found to be important will need to be considered in the simplified equation to predict rotational restraint.

Table 5-1. Summary of parameters influencing rotational restraint

Parameter	Influence
Column Length and Stiffness	Important – directly considered in k-factor equation
Girder Length and Stiffness	Not important – Stiffness of girders is much greater than that of joint
Girder Depth	Not important – Did not change rotational stiffness in model
Bent Cap Length	Important – Stiffness calculated per ft of bent cap length
Connection Interface	Important – Not considered because part of standard practice
Dowel Bar Area	Important – slope of effect 311 kip-ft/rad per in^2 total dowel bar area
Concrete Stiffness	Important – Assume standard 4000 psi concrete use
Diaphragm Width	Important – slope of effect 597 kip-ft/rad per inch diaphragm width
Skew	Important – slope of effect -195 kip-ft/rad per degree skew

Chapter 6: Rotational Restraint and k-factor Design Equations

Utilizing the parametric analysis discussed in **Chapter 5**, a simplified design equation was developed to predict rotational restraint at the top of intermediate bents. Subsequently, a simplified equation for the k-factor was determined. In addition, a design approach for determining the k-factor for telescoping columns was developed. Finally, estimation of the potential for cost savings was explored.

Rotational Restraint Design Equation

The analysis from **Chapter 5** was used to develop a design equation to predict rotational stiffness (R_{kb}). The key parameters, including bent cap length, dowel bar area, diaphragm width, and skew angle are included in the draft simplified equation for rotational stiffness.

$$R_{kb} = 8700 + k_D(A_d - 8) + k_{DW}(D_w - 30) - k_S \times Skew$$

Where:

R_{kb} = the rotational stiffness at the top of column ($kip \cdot ft/rad\ per\ ft\ of\ bent\ cap\ length$)

A_d = the total area of dowel bars in $in.^2$

D_w = the diaphragm width in $in.$

$Skew$ = the skew angle in degrees

k_D = the factor for the dowel bar area

k_{DW} = the factor for the diaphragm width

k_S = the factor for the skew angle

Equation 7. Simplified equation for calculating rotational stiffness (using expected concrete modulus)

Based on the slopes from **Chapter 5**, the k_D factor should be 311, the k_{DW} factor 597, and the k_S factor 195. However, an optimization analysis, that sought to reduce the sum of the squared errors using the seven different FE models, suggested a k_D factor of 324, a k_{DW} factor of 578, and a k_S factor of 144, which are very similar to the slope values. For the ease of design, using the following final suggested factors is proposed:

k_D = 300
k_{DW} = 600
k_S = 150

Table 6-1 shows the seven different models used in the previous parametric analysis along with their key parameters, results of the FE, and the predicted R_{kb} using the suggested factors. The analysis shows that the simplified prediction of the R_{kb} was within 10% of the values obtained from the FE.

The simplified equation uses the base R_{kb} per ft length of bent cap of 8700 $kip \cdot ft/rad$. If the actual diaphragm length is used, then the value becomes 9000 $kip \cdot ft/rad$ per ft width of the diaphragm. The values "8" and "30" are simply the dowel bar area and the diaphragm width of the A8697 bridge that was used to build the base model. Another version of the R_{kb} equation without these constants is:

$$R_{kb} = -11700 + k_D A_d + k_{DW} D_w - k_S \times Skew$$

Where:

R_{kb} = the rotational stiffness at the end b ($kip \cdot ft/rad\ per\ ft\ of\ bent\ cap\ length$)

A_d = the total area of dowel bars in $in.^2$

D_w = the diaphragm width in $in.$

$Skew$ = the skew angle in degrees

k_D = the factor for the dowel bar area

k_{DW} = the factor for the diaphragm width

k_S = the factor for the skew angle

Equation 8. Alternative version of simplified equation for calculating rotational stiffness

However, as mentioned in **Chapter 5,** the FE model utilized a concrete modulus of 4351 ksi based on the tested modulus from A7957, rather than the estimated modulus of 3605 ksi for concrete with a compressive strength of 4000 psi (per ACI 318 19.2.2) or 3644 *ksi* to 3987 *ksi* per AASHTO. This deviation results in a 9% reduction in the predicted R_{kb} values. Therefore, the proposed design equation is revised as follows:

$$R_{kb} = 7900 + k_D(A_d - 8) + k_{DW}(D_w - 30) - k_S \times Skew$$

Where:

R_{kb} = the rotational stiffness at the end b ($kip \cdot ft/rad\ per\ ft\ of\ bent\ cap\ length$)

A_d = the total area of dowel bars in $in.^2$

D_w = the diaphragm width in $in.$

$Skew$ = the skew angle in degrees

k_D = the factor for the dowel bar area

k_{DW} = the factor for the diaphragm width

k_S = the factor for the skew angle

Equation 9. Proposed design equation for calculating rotational stiffness (using design concrete modulus)

In this case, the alternative form of the equation, without the constants is:

$$R_{kb} = -12500 + k_D A_d + k_{DW} D_w - k_S \times Skew$$

Where:

R_{kb} = the rotational stiffness at the end b ($kip \cdot ft/rad\ per\ ft\ of\ bent\ cap\ length$)

A_d = the total area of dowel bars in $in.^2$

D_w = the diaphragm width in $in.$

$Skew$ = the skew angle in degrees.

k_D = the factor for the dowel bar area

k_{DW} = the factor for the diaphragm width

k_S = the factor for the skew angle

Equation 10. Alternative proposed design equation for calculating rotational stiffness

In addition, given the variability of parameters and the need for additional safety margins, a further reduction of 10-20% can be applied. The exact value of the additional safety factor will be determined at the discretion of MoDOT. Designers can then use this R_{kb} value, multiply by the length of the bent cap, and divide by the number of columns in the bent to determine the rotational stiffness at the top of each column.

Table 6-1. Summary of the FE models and R_{kb} predictions

Bridge Model	Parameters				FE Output		Prediction	
	Dowel bar area (in^2)	Bent cap length (ft)	Diaphragm width (in.)	Skew Angle (degrees)	R_{kb} (k-ft/rad)	R_{kb}/bent cap length (k-ft/rad per ft)	R_{kb} Prediction (k-ft/rad per ft)	Difference (%)
A8697	7.92	32	30.0	0.0	277,237	8,664	8,676	0
A7957	10.56	44	40.5	30.0	552,474	12,556	11,268	-10
A8279	4.40	29	34.5	30.0	174,763	6,026	5,820	-3
A8697 w/ 45 skew	8.80	44	46.5	45.0	497,774	11,313	12,090	7
A8697 w/ 22 skew	7.92	35	40.5	22.5	418,361	11,953	11,601	-3
A8697 w/ 33 dowel bars	14.52	32	30.0	0.0	343,044	10,720	10,656	-1
A8697 w/ 42 in. diaphragm	7.92	32	42.0	0.0	506,633	15,832	15,876	0

Estimation of k-factor

With the rotational stiffness at the top of the column (R_{kb}) and the column length and stiffness (EI/L), the k-factor can be determined through **Equation 4**, presented in **Chapter 2**. However, solving this equation may be complicated. Hence, to offer a more manageable solution, an approximate bi-linear solution is given in **Equation 11** and shown in **Figure 6-1**.

$$k\_factor = \begin{cases} 2.000 - 0.3135 \times \dfrac{R_{kb} L}{EI} & for \ \dfrac{R_{kb} L}{EI} < 2 \\ 1.428 - 0.0275 \times \dfrac{R_{kb} L}{EI} & for \ \dfrac{R_{kb} L}{EI} \geq 2 \end{cases}$$

Where:

R_{kb} = the rotational stiffness at the end b ($kip \cdot ft/rad \ per \ ft \ of \ bent \ cap \ length$)

L = the length of the column from point of fixity to top of bent cap

E = the modulus of elasticity of the column

I = the second moment of inertia of the column

Equation 11. Approximate bi-linear equation for k-factor

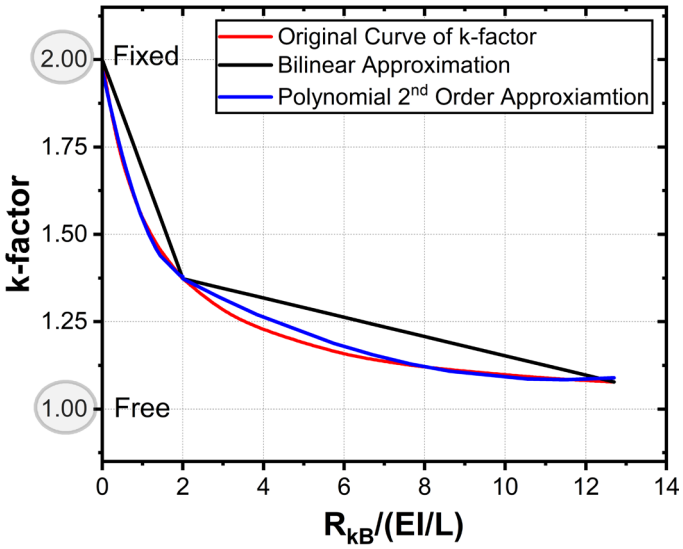

Figure 6-1. Bilinear approximation of k-factor

The bilinear equation does introduce some error in the approximation of the k-factor but is conservative. Another equation, using a polynomial, is shown in **Equation 12**, and displays improved accuracy.

$$k\_factor = \begin{cases} 1.972 - 0.5615\frac{R_{kb}L}{EI} + 0.1327\left(\frac{R_{kb}L}{EI}\right)^2 & for\ \frac{R_{kb}L}{EI} < 2 \\ 1.51 - 0.075\frac{R_{kb}L}{EI} + 0.0033\left(\frac{R_{kb}L}{EI}\right)^2 & for\ \frac{R_{kb}L}{EI} \geq 2 \end{cases}$$

Equation 12. Polynomial approximation of k-factor

Telescoping Columns

The calculation of the k-factor, as presented in **Equation 4**, utilizes the column stiffness (EI) and length (L). However, in the case of telescoping columns, a procedure is needed to determine an equivalent EI/L for the telescoping column. In this case, an equivalent modulus (I_{eq}) is determined so that the buckling analysis can be completed as if the column was not telescoping. Two examples are presented below, using the bent #3 from the A8697 bridge, see **Figure 6-2** and a bent with a longer column.

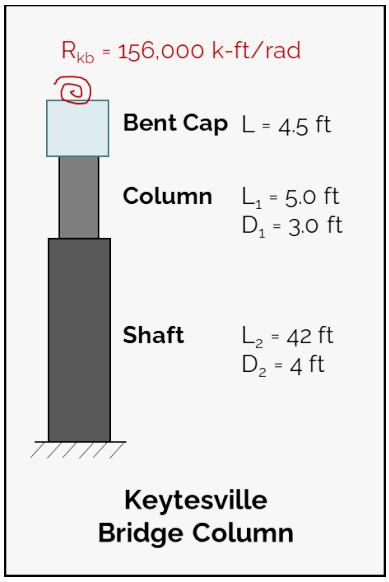

Figure 6-2. Analysis of telescoping column – Example 1

Example 1

Step 1 – Determine the predicted rotational restraint.

The bridge plans for A8697 show the following:
Dowel bar area A_d = 18*0.44 $in.^2$ = 7.92 $in.^2$
Diaphragm width, D_w = 30 $in.$
Skew = 0 degrees
Bent cap length = 32 ft

**note – this example assumed that the dowel bars can be fully developed. Designers should check that the dowel bars can develop design stresses with specified embedment length or provide the full development length. For this bridge under test loads of Chapter 4, the stress in the bars was only 10 ksi.*

Using **Equation 9** with k_D = 300, k_{DW} = 600, k_S = 150; R_{kb} = 7876 $kip \cdot ft/rad$ per ft bent cap length.

The total rotational stiffness at the top of the column is:
$Total\ R_{kb} = R_{kb}\ per\ bent\ cap\ length \times Bent\ Cap\ length = 7876 \times 32\ ft = 252{,}032\ kip \cdot ft/rad$

Since the bent has two columns, the rotational stiffness is shared between them. Therefore, the stiffness at the top of each column is 126,016 $kip \cdot ft/rad$.

Step 2 – Determine the buckling load for a telescoping column with no rotational restraint.

The bridge plans show that the length of the shaft to assumed depth of fixity is 41 ft (assumed to be at the top of the rock elevation in this example), the length of the column is 6’ 7 ¼”, and

the bent cap height is 4.5 ft. The column is 3 ft diameter and the shaft is 4 ft diameter. This gives a moment of inertia for the column (I_1) of 3.97 ft^4, and for the shaft (I_2) of 12.56 ft^4.

According to MoDOT EPG 751.31.2.4, the predicted buckling capacity (P_c) is 9,879 kip. However, this equation is inaccurate for telescoping columns with relatively short columns. An alternative equation in (Timoshenko & Gere, 1962) (**Equation 13**) gives the capacity to be 8494 kip.

$$P_{cr} = \frac{\pi^2 E I_2}{4l^2} \frac{1}{\frac{l_2}{l} + \frac{l_1}{l}\frac{I_2}{I_1} - \frac{1}{\pi}\left(\frac{I_2}{I_1} - 1\right)\sin\frac{\pi l_2}{l}} = \mathbf{8,494\ kip}$$

Equation 13. Critical buckling load according to (Timoshenko & Gere, 1962)

Step 3 – Determine the equivalent moment of inertia (I_{eq}) of a non-telescoping column that would give the same buckling capacity.

Using an E value of 4351 ksi and a total length of 47.6 ft the equivalent moment of inertia (I_{eq}) is 12.45 ft^4, using **Equation 14**.

$$I_{eq} = \frac{P_c 4L^2}{E\pi^2}$$

Equation 14. Equivalent moment of inertia for telescoping columns

**note – In this example both the shaft and upper column have the same E value. If the concrete strengths differ a weighted average (based on the length of the sections as shown below) for the modulus can be used. The modulus of elasticity of the shaft may be adjusted for the presence of steel casing, but no recommendation is made from this research.*

$$E_{eff} = \frac{\sum(l_n E_n)}{L}$$

E_n = modulus of elasticity for column segment n

The height of the bent cap (4.5 ft) can be added to the length to give a total L of 52.1 ft. This gives the equivalent non-telescoping column an EI_{eq}/L of:

$$\frac{EI_{eq}}{L} = \frac{626562\ ksf * 12.45\ ft^4}{52.1} = 149{,}605\ k \cdot ft$$

Step 4 – Determine k-factor and buckling capacity.

Using **Equation 11** with an R_{kb} = 126,016 $kip \cdot ft/rad$ and an EI/L_{eq} of 149,605 $kip \cdot ft$, the k-factor becomes 1.74. If **Equation 4** is used, then the k-factor would be 1.59.

With a k-factor of 1.74, using Euler's buckling equation the buckling capacity (P_c) of the telescoping column would be:

$$P_c = \frac{\pi^2 E I_{eq}}{(kL^2)} = 9{,}367\ kip$$

With a k-factor of 1.59, using Euler's buckling equation the buckling capacity (P_c) of the telescoping column would be:

$$P_c = \frac{\pi^2 E I_{eq}}{(kL^2)} = \ 11{,}200\ kip$$

The difference in the k-factor between the bilinear approximation (**Equation 11**) and the exact equation (**Equation 4**) does result in an 18% difference in the buckling capacity.

An analysis using SAP 2000 yields a buckling capacity of 11,290 kip for the partially restrained telescoping column, which is very close to the solution using the exact k-factor of 1.59.

Also of note is that the buckling capacity of the column with no rotational restraint (with an extra 4.5 ft for the bent cap height), as per **Equation 13**, would be 7,106 kip. This value is 24% lower than the capacity calculated using the bilinear k-factor (9,367 kip) and 36% lower than the capacity calculated using the theoretical k-factor (11,200 kip). The increase in buckling capacity by including the rotational restraint may help to reduce the size of the column if other design criteria do not control.

Example 2

Another example of the same column, except with the lengths of the shaft and column changed per **Figure 6-3** is also given.

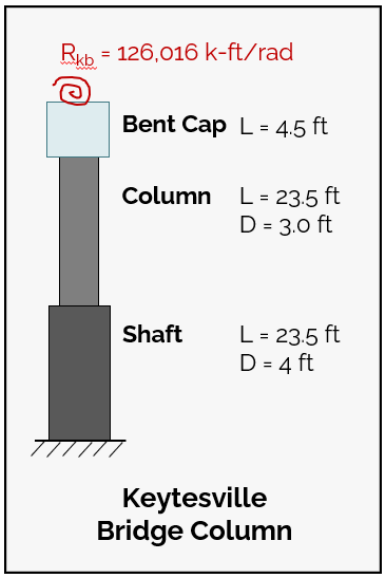

Figure 6-3. Analysis of telescoping column – Example 2

Step 1 – Determine the predicted rotational stiffness.

The bridge plans for A8697 show the following:
Dowel bar area A_d = 18*0.44 $in.^2$ = 7.92 $in.^2$
Diaphragm width, D_w = 30 $in.$
Skew = 0 degrees
Bent cap length = 32 ft

Using **Equation 9** with k_D = 300, k_{DW} = 600, k_S = 150; R_{kb} = 7876 $kip \cdot ft/rad$ per ft bent cap length

The total rotational stiffness at the top of the column is:
$Total\ R_{kb} = R_{kb}\ per\ bent\ cap\ length \times Bent\ Cap\ length$ = 7876 × 32 ft = 252,032 $kip \cdot ft/rad$

Since the bent has two columns, the rotational stiffness is shared between them. Therefore, the stiffness at the top of each column is 126,016 $kip \cdot ft/rad$

Step 2 – Determine the buckling load for a telescoping column with no rotational restraint.

The length of the shaft to assumed depth of fixity is 23.5 ft, the length of the column is 23.5 ft, and the bent cap height is 4.5 ft. The column is 3 ft diameter, and the shaft is 4 ft diameter.

According to MoDOT EPG 751.31.2.4, the predicted buckling capacity (P_c) is 6,515 kip. An alternative equation in (Timoshenko & Gere, 1962) (**Equation 13**) gives the capacity to be 6315 kip which is much closer to the MoDOT EPG equation for this case of relatively equal column and shaft lengths.

Step 3 – Determine the equivalent moment of inertia (I_{eq}) of a non-telescoping column that would give the same buckling capacity.

Using an E value of 4351 ksi and the length of 47 ft the equivalent moment of inertia (I_{eq}) is 9.02 ft^4, using **Equation 14**.

The height of the bent cap (4.5 ft) can be added to the length to give a total L of 51.5 ft. This gives the equivalent non-telescoping column an EI_{eq}/L of

$$\frac{EI_{eq}}{L} = \frac{626562\ ksf * 9.02\ ft^4}{51.5} = 109{,}739\ kip \cdot ft$$

Step 4 – Determine k-factor and buckling capacity.

Using **Equation 11** with an R_{kb} = 126,016 $kip \cdot ft/rad$ and an EI/L_{eq} of 109,739 $kip \cdot ft$, the k-factor becomes 1.64. If **Equation 4** is used, then the k-factor would be 1.56.

With a k-factor of 1.64, using Euler's buckling equation the buckling capacity (P_c) of the telescoping column would be:

$$P_c = \frac{\pi^2 EI_{eq}}{(kL^2)} = 7{,}821\ kip$$

With a k-factor of 1.56, using Euler's buckling equation the buckling capacity (P_c) of the telescoping column would be:

$$P_c = \frac{\pi^2 EI_{eq}}{(kL^2)} = 8{,}845\ kip$$

An analysis using SAP 2000 yields a buckling capacity of 9,864 kip for the partially restrained telescoping column.

The SAP solution shows a slightly greater difference in **example 2** compared to **example 1**; however, the estimation for the telescoping column is still within 10%. Notably, the capacity of the partially restrained column is 40% greater than the capacity of the unrestrained column (5614 kip with bent cap included).

H-Pile Column

To investigate the procedure with H-pile columns, the buckling capacity of the columns in bridge A8279 is analyzed. The strong axis is arranged parallel to the bent and the weak axis arranged perpendicular to the bent.

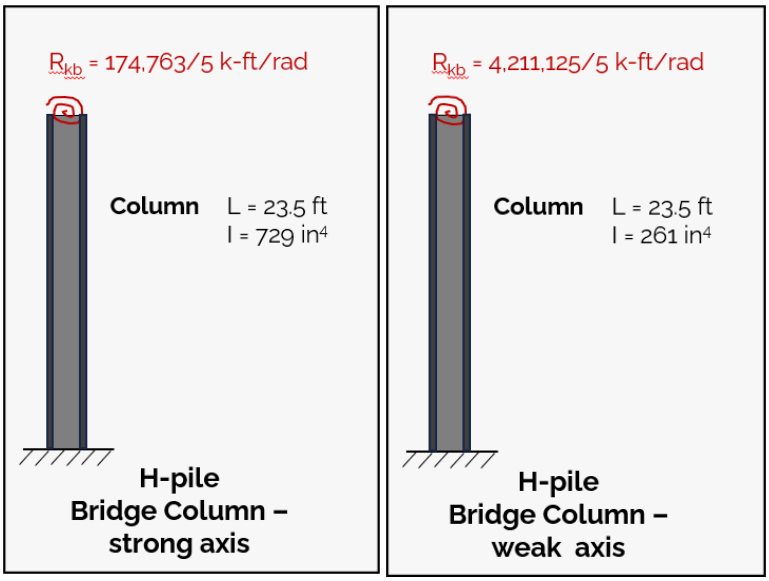

Figure 6-4. Analysis of HP column

Step 1 – Determine the predicted rotational restraint.

The bridge plans for A8279 show the following:
HP 14x73 piles with I_x 729 in^4 = and I_y = 261 in^4
Diaphragm width, D_w = 34.5 $in.$
Skew = 30 degrees
Bent cap length = 29 ft

Using **Equation 9** with k_D = 300, k_{DW} = 600, k_S = 150; R_{kb} = 5020 $kip \cdot ft/rad$ per ft bent cap length, the total rotational stiffness at the top of the column is:

$Total\ R_{kb} = R_{kb}\ per\ bent\ cap\ length \times Bent\ Cap\ length =$ 5020 × 29 ft = 145,580 $kip \cdot ft/rad$

Since the bent has five columns, each column shares the rotational stiffness. Therefore, the restraint at the top of each column is 29,116 $kip \cdot ft/rad.$

The bridge plans show that the column is 23.5 ft long with a strong axis I of 729 $in.^4$ and a weak axis I of 261 $in.^4$. This is a non-telescoping column, so the length remains at 23.5 ft.

Step 2 – Determine k-factor and buckling capacity.

Using **Equation 11** with an R_{kb} = 29,116 $kip \cdot ft/rad$ and an EI/L of 6247 $kip \cdot ft$, the k-factor becomes 1.30. If **Equation 4** is used, then the k-factor would be 1.19.
With a k-factor of 1.30, using Euler's buckling equation the buckling capacity (P_c) of the telescoping column would be:

$$P_c = \frac{\pi^2 EI}{(kL^2)} = \ 1{,}553\ kip$$

With a k-factor of 1.19, using Euler's buckling equation the buckling capacity (P_c) of the telescoping column would be:

$$P_c = \frac{\pi^2 EI}{(kL_{eq}^2)} = \ 1{,}840\ kip$$

An analysis using SAP 2000 yields a buckling capacity of 1,792 kip for the partially restrained column, which is very close to the solution.

If no rotational restraint were considered, then the capacity would only be 656 kip. The inclusion of rotational restraint in this case results in a 62% increase in buckling capacity.

In addition, the FE model showed that the rotational restraint at the top of the HP pile in the weak axis is 4,211,000 $kip \cdot ft/rad$. This is essentially a fixed connection and would use a theatrical k-factor of 1.0 (current MoDOT practice is to assume the fixed connection in the plane of the bent). The buckling capacity in this direction would be 945 kip.

The consideration of the rotational restraint means that the columns are controlled by the weak axis buckling with a capacity of 945 kip, but this is still 44% greater than the case with no assumed rotational restraint in the strong axis (656 kip). Additional weak axis capacity could be achieved with the addition of bracing to make this design even more cost effective.

Comparison of k-factors

For the bridges presented in **Table 6-1**, a comparison is made between the k-factor determined through the predicted R_{kb}using **Equation 7** and the R_{kb}obtained from the FE model. The k-factor uses the bilinear approximation in **Equation 11**. Note – the prediction uses the E value as used in the FE models rather than the reduced E value for 4000 psi concrete.

The results, shown in **Table 6-2**, indicate that the use of the prediction equation for R_{kb} results in at most a 6% difference in the k-factor and a 12% difference in the buckling load (P_c). In addition, the new k-factors are much less than 2.0 in most cases with the greatest difference occurring in the steel column bridge, in which the k-factor was reduced to 1.30.

Table 6-2. Comparison of k factors and P_c for model and predicted R_{kb}

Bridge Model	FE Output		Prediction		FE k-factors		Prediction k-factor		% Difference FE vs. Prediction	
	R_{kb} (k-ft/rad per ft)	R_{kb}/ (EIeq/L)	R_{kb} (k-ft/rad per ft)	R_{kb}/ (EIeq/L)	k-factor	Pcr (kip)	k-factor	Pcr (kip)	k-factor	Pcr (kip)
A8697	8664	0.838	8676	0.92	1.74	9485	1.71	9767	1.45	2.97
A7957	12556	1.538	11268	1.47	1.52	9603	1.54	9355	-1.32	-2.58
A8279	6026	5.595	5820	5.40	1.21	1795	1.28	1603	-5.82	-10.7
A8697 w/ 45 skew	11313	1.505	12090	1.77	1.53	12153	1.45	13578	5.39	11.72
A8697 w/ 22 skew	11953	1.265	11601	1.35	1.60	11039	1.58	11413	1.65	3.39
A8697 w/ 33 dowel bars	10720	1.037	10656	1.13	1.67	10118	1.64	10492	1.80	3.70
A8697 w/ 42 in. diaphragm	15832	1.531	15876	1.69	1.52	12287	1.47	13121	3.23	6.79

Suggested Design Procedure

Following the results of the previous section, a design procedure to include the effect of the rotational restraint at the top of the columns can be established. This will result in the k-factor that can be used in the same way as the current 2.1 factor that is used in MoDOT EPG 751.31.2.4. In this design procedure, the k factor is used for the buckling capacity and slenderness check.

Step 1 – Determine the predicted rotational restraint per ft of the bent cap using **Equation 9.**

$$R_{kb} = 7900 + k_D(A_d - 8) + k_{DW}(D_w - 30) - K_S \times Skew$$

Where:

R_{kb} = is the rotational stiffness at the end b ($k \cdot ft/rad\ per\ ft\ of\ bent\ cap\ length$)

A_d = is the total area of dowel bars in $in.^2$

D_w = is the diaphragm width in $in.$

$Skew$ = is the skew angle in degrees

k_D = is the factor for the dowel bar area

k_{DW} = is the factor for the diaphragm width

k_S = is the factor for the skew angle

This value of rotational restraint may be multiplied by an additional safety factor to account for the variation in the restraint level compared to the FE model results. Given that the error between the FE model and prediction was ~10%, an additional factor of 0.9 may be applied.

The rotational restraint is based on the assumption of fully bonded dowel bars. The design may either check the dowel bar stresses under design loads to ensure proper embedment length, or embed the dowel bars the full development length.

The rotational restraint R_{kb} should be multiplied by the bent cap length and divided by the number of columns in the bent to achieve the restraint at the top of each column.

$$R_{kb-col} = \frac{R_{kb} * bent\ cap\ length}{\#\ columns\ in\ bent}$$

Equation 15. Rotational stiffness per column

The equation for rotational restraint assumes that the dowel bars are fully bonded to the concrete. Designers should check that the stress in the bar under design loads can be developed with the given embedment length or provide the full development length of the bars.

Step 2 – Determine the buckling load for a telescoping column with no rotational restraint.

For the case of telescoping columns, an approximation is needed to determine the buckling capacity. First the capacity of a telescoping column with no rotational restraint at the top can be determined through MoDOT EPG 751.31.2.4 or **Equation 13**, with the latter being more accurate for cases of unequal segment length.

Step 3 – Determine the equivalent moment of inertia (I_{eq}) of a non-telescoping column that would give the same buckling capacity using **Equation 14**.

$$I_{eq} = \frac{P_c 4L^2}{E\pi^2}$$

Step 4 – Determine k-factor

Use the bilinear approximation to determine the k-factor per **Equation 11**.

$$k\_factor = \begin{cases} 2.000 - 0.3135 \times \frac{R_{kb-col} L}{EI_{eq}} & for \ \frac{R_{kb-col} L}{EI_{eq}} < 2 \\ 1.428 - 0.0275 \times \frac{R_{kb-col} L}{EI_{eq}} & for \ \frac{R_{kb-col} L}{EI_{eq}} \geq 2 \end{cases}$$

Where:

R_{kb-col} = the rotational stiffness at the end b ($k \cdot ft/rad \ per \ ft \ of \ bent \ cap \ length$)

L = the length of the column (to top of bent cap)

E = the modulus of elasticity of the column (see note)

I_{eq} = the equivalent second moment of inertia of the column

Note - The modulus of elasticity should be the expected modulus (~1.2 times the design) for this calculation. A higher stiffness in the columns will lead to a larger k-factor and a more conservative solution. If two elements (column and shaft) have different moduli, then use the greater value.

Step 5 – Adjustment for k-factor

Even in the case of no rotational restraint, the theoretical k-factor of 2.0 is adjusted to 2.1 for design. A similar adjustment should be applied to the k-factors calculated with partial rotational restraint.

$$K_{design,x} = \frac{2.1 \times k\_factor}{2.0}$$

Equation 16. Design k-factor

Step 6 – Determine buckling capacity

The buckling capacity of the column can then be determined through the standard Euler buckling equation with the new design k-factor. For this equation, the design modulus can be used.

$$P_c = \frac{\pi^2 E I_{eq}}{(kL^2)}$$

Cost Savings

Including rotational restraint at the top of the bridge column may result in potential cost savings if the buckling capacity controls the design. The previous examples showed that including rotational restraint increased the buckling capacity by 24% to 40%. This enhanced capacity could potentially allow for the optimization of column sizes, consequently reducing material costs.

Example 1

The first example considers bridge A8279 with HP columns. As detailed previously, the inclusion of rotational restraint (without safety factors applied) would result in a buckling capacity of 1716 kip in the strong axis, which is 62% greater than the capacity with no rotational restraint (k=2.0) of 656 kip. This means that the weak axis (with a fixed column top) would control the design with a capacity (k=1.0) of 945 kip.

Assuming that the capacity of 656 kip controlled the design, a design that utilizes rotational restraint and gives the weak axis capacity of 656 kip would only require an I_y of 182 $in.^4$. However, in this case, the next lighter section would only have a I_y of 153 $in.^4$ so the same size column would still be used. However, it may be possible to use a fewer number of columns. If the original design (with no rotational restraint) needed 656 kip x 5 columns = 3280 kip. Then the design with rotational restraint and a 945 kip capacity would only need 4 columns, resulting in approximately a 20% reduction cost per bent.

Example 2

For the second example with the bridge A8697 with altered column length of 23.5 ft and shaft length of 23.5 ft the column capacity with restraint was 7,821 kip and without restraint was 6315 kip. If no other criteria controlled the design, then the column diameter could be reduced to 2.2 ft to achieve the buckling capacity of 6315 kip. Dropping from a 3' column to a 2.5' column is a 30% reduction in area/volume and would result in a similar reduction in column cost when cost of concrete, rebar and labor are factored in.

Summary

A simplified equation was developed to predict the rotational restraint at the top of intermediate bents. The factors in the equation consider the key parameters, including dowel bar area, diaphragm width, and skew angle. The suggested factors align well with the slope values found in **Chapter 5**. A comparison between the predicted rotational stiffness and that obtained from the FE models shows that the rotational stiffness can be estimated to be within a 10% margin. In addition, the theoretical relationship between the k-factor and the rotational stiffness and column flexural stiffness was simplified into a bilinear or bi-polynomial equation. Calculations of the k-factors for the modeled bridges showed k-factors less than the assumed 2.0, with the steel column bridge showing a particularly low k-factor of only 1.30. A procedure for analyzing telescoping columns has been formulated, in which an effective moment of inertia can be used to treat the column as having a uniform diameter. Three examples demonstrated that the use of rotational restraint increased the buckling capacity of the column by 24% to 40%. For steel HP columns, this increase was most significant at 62%, which changed the controlling buckling mode to the weak axis direction. The increase strength may result in a cost savings of 20% to 30% based on the presented examples if no other criteria (other than

buckling capacity) control the design. The chapter culminates with a suggested design procedure for including rotational restraint in the design of intermediate bent bridge columns.

Chapter 7: Summary and Conclusions

This report provides a thorough investigation of the restraint at the top of the column of non-integral intermediate bents with closed diaphragms, with a focus on a common connection configuration utilized by MoDOT. Although closed diaphragms inherently possess some level of rotational restraint, the current design approach considers this type of connection as free, resulting in the use of design k-factors of 2.1. However, restraint arises from the diaphragm width and the area of dowel bars. This rotational restraint significantly influences the k-factor. Utilizing an integration of experimental and numerical analyses, the study determined the accurate level of restraint of these types of intermediate bents and developed a procedure to consider restraint in design.

In this study, a thorough literature review was conducted of the rotational stiffness, field testing, numerical modeling, and buckling analysis of the bent column joint.

To investigate the rotational restraint, detailed FE models (bridges A7957, A8697, and A8279) were created using ANSYS workbench. The detailed FE models considered the standard design details including the shear keys, dowel bars, roofing felt bond breaker between the diaphragm and bent cap, and joint filler. The A8697 bridge and the A7957 bridge were used for the FE validation.

Experimental testing was conducted on bridge A8697 via loaded dump trucks. The movements of the bridge were recorded via DIC and LVDTs. The DIC data showed good accuracy in the horizontal direction but was less accurate in the vertical direction due to possible movements in the camera. The DIC rotation data showed that the girder and diaphragm rotated together, with about 10 times more rotation than the bent cap. This observation was consistent with the FE model results, indicating most of the rotational flexibility was attributed to the bent cap to diaphragm connection. The LVDT data were consistent across all three test runs and reasonably matched the FE predictions for the deflections of the bent cap and loaded side girder. Overall, the experimental results verified the accuracy of the FE model.

A parametric analysis was performed to determine the influence of several key parameters on the rotational restraint at the top of intermediate bent columns. The results showed that the dowel bar area, diaphragm width, and skew angle were all parameters that needed to be considered in the simplified equation to predict the rotational stiffness. Conversely, the girder length and stiffness were not crucial factors. Additionally, the connection interface was assumed to be part of standard design practice and if changed would require revisiting the recommended simplified equation parameters. The dowel bars were assumed to be fully bonded to the concrete. A designer may need to check the stress in the bars under design loads to ensure development or provide full development length. The concrete modulus was identified as an important parameter, but it was considered to be a constant for 4000 psi concrete. Meanwhile, the column length and stiffness, as well as the bent cap length, were directly considered in the formulation of the k-factor equation.

A simplified equation has been developed to predict the rotational stiffness at the top of intermediate bents. The suggested factors for dowel bar area, diaphragm width, and skew angle match well with the slope values found in **Chapter 5**. A comparison of the predicted rotational stiffness to that found in the FE models shows that the rotational stiffness can be estimated within a 10% margin. In addition, the theoretical relationship between the k-factor and the rotational stiffness and column flexural stiffness was simplified into a bilinear equation. Calculations of the k-factors for the modeled bridges showed k-factors less than the assumed 2.0 (on average 1.5), with the steel column bridge showing a particularly low k-factor of only 1.30. A procedure for analyzing telescoping columns was also formulated in which the effect of the moment of inertia can be used to treat the column as having a uniform diameter. Three examples showed that the use of rotational restraint increased the buckling capacity of the concrete column by 24% to 40%. For steel HP columns, this increase was most significant at 62%, which changed the controlling buckling mode to the weak axis direction.

The work culminates in a suggested design procedure to use rotational restraint in the design of intermediate-bent bridge columns.

References

Abdalla, O. A., Ramirez, J. A., & Lee, R. H. (1993). *Strand debonding in pretensioned beams-Precast prestressed concrete bridge girders with debonded strands-Continuity issues*.

Astaneh, A., Bergsma, G., & Shen, J. H. (1992). Behavior and design of base plates for gravity, wind and seismic loads. *Proceedings of the National Steel Construction Conference*, 209–214.

Balut, N., & Moldovan, A. (1997). A model for the behavior of column base connections. *Proceedings of the Second Conference STESSA, Kyoto, Japan*.

Bell, E. S., Gaylord, D., Goudreau, A., White, D., & others. (2015a). *Instrumentation, digital image correlation, and modeling to monitor bridge behavior and condition assessment.*

Bell, E. S., Gaylord, D., Goudreau, A., White, D., & others. (2015b). *Instrumentation, digital image correlation, and modeling to monitor bridge behavior and condition assessment.*

Brun, P. (1976). *Etude d'un assemblage imparfaitement rigide et des effets de sonutilisations dans un multi-étagé*. Universite Laval.

Clark, L. A., & Sugie, I. (1997). SERVICEABIILTY LIMIT STATE ASPECTS OF CONTINUOUS BRIDGES USING PRECAST CONCRETE BEAMS. *Structural Engineer*, *75*(11).

Dantec Dynamics. (2018). *Basic User Training Course 1.0*.

Desai, N. (2016). Small-strain measurement in bridge connections using the digital image correlation (DIC) technique. *Health Monitoring of Structural and Biological Systems 2016*, *9805*, 752–769.

Duan, L., & Chen, W. F. (1999). Effective length factors of compression members. *Structural Engineering Handbook*.

Ermopoulos, J. C., & Stamatopoulos, G. N. (1996). Analytical modelling of column-base plates under cyclic loading. *Journal of Constructional Steel Research*, *40*(3), 225–238.

FIB Task Group on Bond Models. (2000). *Bond of Reinforcement in Concrete*.

Gomez, I., Kanvinde, A., & Deierlein, G. G. (2010). Exposed column base connections subjected to axial compression and flexure. *AISC, Chicago*, *257*.

Grauvilardell, J. E., Lee, D., Hajjar, J. F., & Dexter, R. J. (2005). Synthesis of design, testing and analysis research on steel column base plate connections in high-seismic zones. *Structural Engineering Report No. ST-04-02. Minneapolis (MN): Department of Civil Engineering, University of Minnesota*.

Hanson, N. W. (1960). *Precast-prestressed concrete bridges: 2. Horizontal shear connections*. Portland Cement Association, Research and Development Laboratories Skokie~….

Hastak, M., Mirmiran, A., Miller, R., Shah, R., & Castrodale, R. (2003). State of practice for positive moment connections in prestressed concrete girders made continuous. *Journal of Bridge Engineering*, *8*(5), 267–272.

Hernandez, E. S., & Myers, J. J. (2016). *FIELD LOAD TEST AND GIRDER DISTRIBUTION FACTORS OF MISSOURI BRIDGE A7957*. https://doi.org/10.13140/RG.2.1.1086.7924

Holombo, J., Priestly, M. J. N., & Seible, F. (2000). Continuity of precast prestressed spliced-girder bridges under seismic loads. *PCI Journal*, *45*(2).

Hou, G., & Chen, S. (2017). Bent connection options for curved and skewed SMC bridges in low-to-moderate seismic regions. *Practice Periodical on Structural Design and Construction*, *22*(4), 4017011.

Jaspart, J.-P., & Vandegans, D. (1998). Application of the component method to column bases. *Journal of Constructional Steel Research*, *48*(2–3), 89–106.

Kaar, P. H., Kriz, L. B., & Hognestad, E. (1960). *Precast-prestressed concrete bridges: 1. Pilot tests of continuous girders*. Portland Cement Association, Research and Development Laboratories.

Kanvinde, A. M., Grilli, D. A., & Zareian, F. (2012a). Rotational stiffness of exposed column base connections: Experiments and analytical models. *Journal of Structural Engineering*, *138*(5), 549–560.

Kanvinde, A. M., Grilli, D. A., & Zareian, F. (2012b). Rotational stiffness of exposed column base connections: Experiments and analytical models. *Journal of Structural Engineering*, *138*(5), 549–560.

Mattock, A. H. (1961). Precast-Prestressed Concrete Bridges. *Journal of the PCA Research and Development Laboratories*.

Melchers, R. E. (1992). Column-base response under applied moment. *Journal of Constructional Steel Research*, *23*(1–3), 127–143.

Menetrey, P., & Willam, K. J. (1995). Triaxial failure criterion for concrete and its generalization. *Structural Journal*, *92*(3), 311–318.

Miller, R. A. (2004). *Connection of simple-span precast concrete girders for continuity* (Vol. 519). Transportation Research Board.

Missouri Department of Transportation. (2023). *Engineering Policy Guide 751.31*.

Murray, C. (2013a). *Dynamic monitoring of rail and bridge displacements using digital image correlation*. Queen's University (Canada).

Murray, C. (2013b). *Dynamic monitoring of rail and bridge displacements using digital image correlation*. Queen's University (Canada).

Nielson, B. G. (2005). *Analytical fragility curves for highway bridges in moderate seismic zones*. Georgia Institute of Technology.

Nielson, B. G., & DesRoches, R. (2007). Seismic performance assessment of simply supported and continuous multispan concrete girder highway bridges. *Journal of Bridge Engineering*, *12*(5), 611–620.

Nonis, C., Niezrecki, C., Yu, T.-Y., Ahmed, S., Su, C.-F., & Schmidt, T. (2013). Structural health monitoring of bridges using digital image correlation. *Health Monitoring of Structural and Biological Systems 2013*, *8695*, 51–63.

Nowak, A. S., & Szerszen, M. M. (2003). Calibration of design code for buildings (ACI 318): Part 1—Statistical models for resistance. *Structural Journal*, *100*(3), 377–382.

Peggar, R. (2014). *Two integral girder connections for precast concrete bridges in seismic regions utilizing extended prestressing strands*.

Picard, A., & Beaulieu, D. (1985a). Behaviour of a simple column base connection. *Https://Doi.Org/10.1139/L85-013*, *12*(1), 126–136. https://doi.org/10.1139/L85-013

Picard, A., & Beaulieu, D. (1985b). Behaviour of a simple column base connection. *Canadian Journal of Civil Engineering*, *12*(1), 126–136.

Salmon, C. G., Schenker, L., & Johnston, B. G. (1957). Moment-rotation characteristics of column anchorages. *Transactions of the American Society of Civil Engineers*, *122*(1), 132–154.

Salmons, J. R. (1974). *End connections of pretensioned I-Beam bridges*.

Salmons, J. R., & McCrate, T. E. (1973). *Bond of untensioned prestress strand*.

Sato, K. (1987). *A Research on the Aseismic Behaviour of Steel Column Base for Evaluating Its Strength Capacity and Fixity*. Kajima Institute of Construction Technology Tokyo, Japan.

Snyder, R. M. (2010). *Seismic performance of an I-girder to inverted-T bent cap bridge connection*. Iowa State University.

Tadros, M. K., Ficenec, J. A., Einea, A., & Holdsworth, S. (1993). A new technique to create continuity in prestressed concrete members. *PRECAST/PRESTRESSED CONCRETE INSTITUTE. JOURNAL*, *38*(5).

Thonstad, T., Eberhard, M. O., & Stanton, J. F. (2021). Design of prestressed, jointed columns for enhanced seismic performance. *Structures*, *33*, 1007–1019.

Timoshenko, S. P., & Gere, J. M. (1962). *Theory of elastic stability*. Courier Corporation.

Wald, F., Sokol, Z., & Steenhuis, M. (1996). Proposal of the stiffness design model of the column bases. In *Connections in Steel Structures III* (pp. 249–258). Elsevier.

Zhao, J., & Sritharan, S. (2007). Modeling of strain penetration effects in fiber-based analysis of reinforced concrete structures. *ACI Structural Journal*, *104*(2), 133.

Appendix A: DIC Results

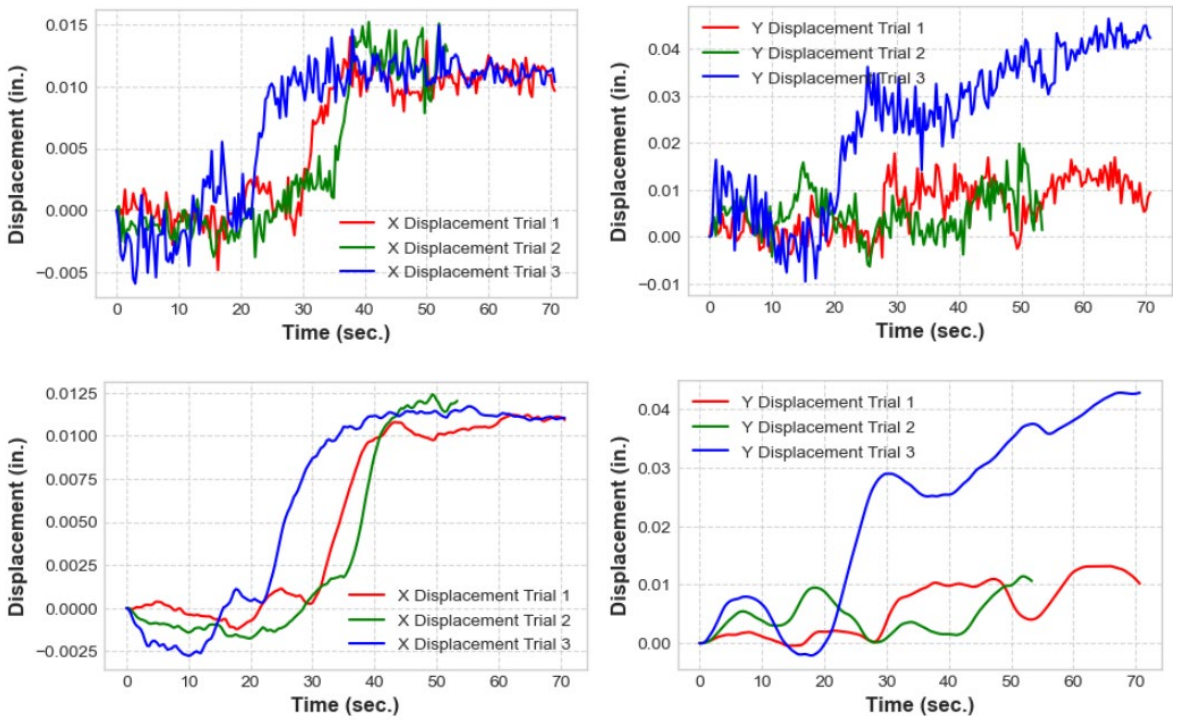

Figure A-1. DIC displacements of the bent cap (raw versus filtered data)

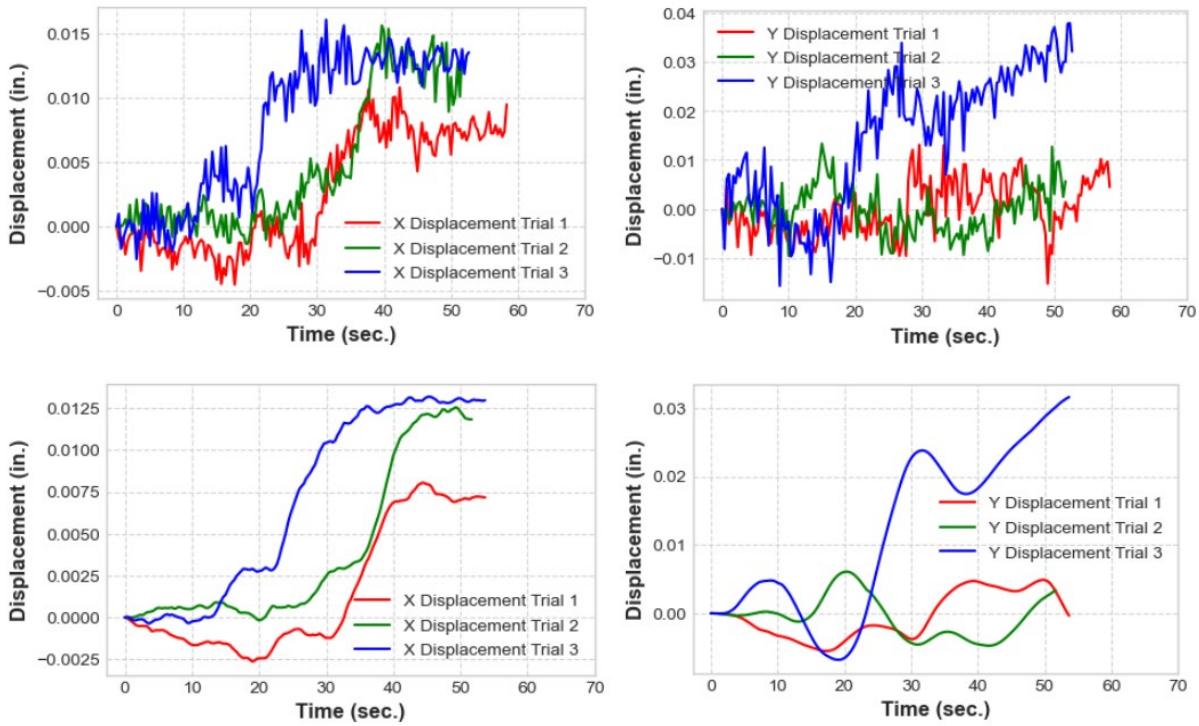

Figure A-2. DIC displacements of the diaphragm (raw versus filtered data)

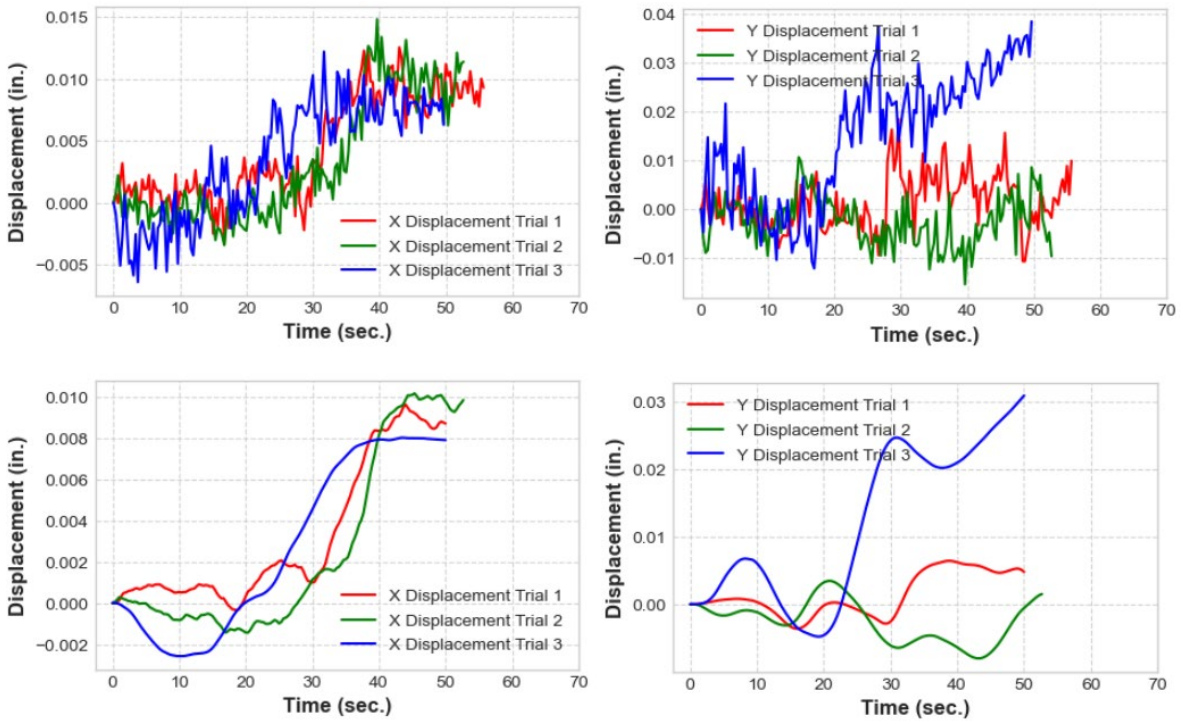

Figure A-3. DIC displacements of the girder (raw versus filtered data)